CHALMERS
UNIVERSITY OF TECHNOLOGY

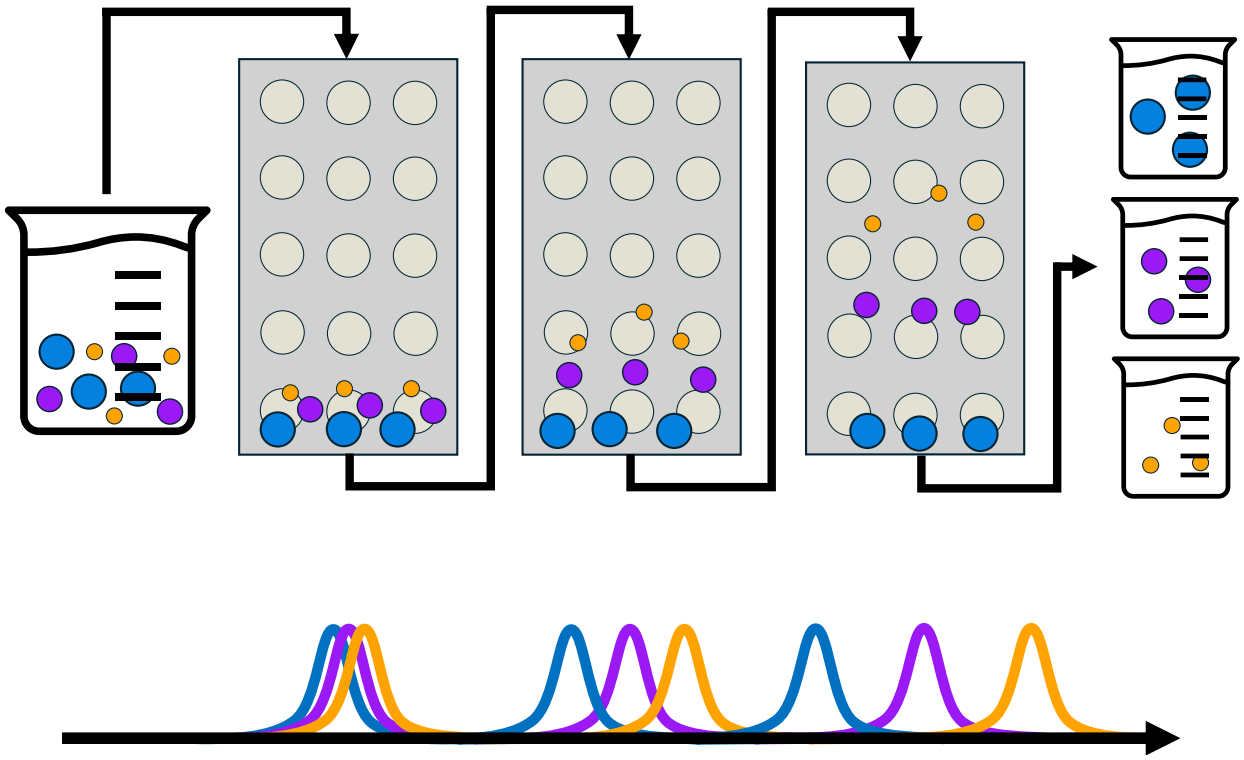

Improving polymeric organic semiconductors through liquid chromatography

Master's thesis in Materials chemistry

SEBASTIAN MÜLLER

DEPARTMENT OF CHEMISTRY AND CHEMICAL ENGINEERING
CHALMERS UNIVERSITY OF TECHNOLOGY
Gothenburg, Sweden 2025
www.chalmers.se

Master's thesis 2025

Improving polymeric organic semiconductors through liquid chromatography

SEBASTIAN MÜLLER

CHALMERS
UNIVERSITY OF TECHNOLOGY

Department of Chemistry and Chemical Engineering
Division of Applied Chemistry
Giovannitti group
Chalmers University of Technology
Gothenburg, Sweden 2025

Improving polymeric organic semiconductors through liquid chromatography
SEBASTIAN MÜLLER

Supervisor: Megan Westwood
Examiner: Alexander Giovannitti

Master's Thesis 2025
Department of Chemistry and Chemical Engineering
Division of Applied Chemistry
Giovannitti group
Chalmers University of Technology
SE-412 96 Gothenburg
Telephone +46 31 772 1000

Cover: Schematic of a HPLC separation

Typeset in LaTeX
Gothenburg, Sweden 2025

Improving polymeric organic semiconductors through liquid chromatography

SEBASTIAN MÜLLER
Department of Chemistry and Chemical Engineering
Chalmers University of Technology

Abstract

Polymeric organic semiconductors (OSCs) are a promising substitute to scarce metals in electronic devices. However, batches are often highly disperse and with variations in their molecular weight (MW) distributions. Moreover, their stiff backbones cause overestimations when measuring their MW relative to typical standards. To overcome this challenge, this project aimed to investigate the use of preparative high-performance liquid chromatography (HPLC) to isolate fractions of polymeric OSCs with narrow dispersities and varying MWs. A method was developed using *poly(3-hexylthiophene)* (P3HT) and subsequently applied to *polydioctylfluorene* (PFO), with the intention of using the latter as an alternative calibration standard.

After optimization, the method demonstrated high reproducibility for P3HT and successfully produced narrow-dispersity fractions for both polymers. Future work should explore the suitability of the obtained PFO fractions as calibration standards.

Keywords: HPLC, SEC, GPC, semiconductive polymers, P3HT, PFO, dispersity, persistence length, NMR.

Acknowledgements

I would like to express my deepest appreciation to my supervisor, Megan Westwood, who has been immensely involved in my project. Despite her busy schedule, she always made time to check in regularly to offer me support and guidance. Her extensive knowledge and enthusiasm greatly inspired me and enabled me to learn a lot during this work.

I am also extremely grateful to my examiner, Alexander Giovannitti. His dedication to my project and helpful advice throughout the course of my work has been invaluable, and greatly improved the quality of this thesis. I am thankful for the opportunity to join his research group, where his outstanding leadership encouraged an inspiring and collaborative environment, making this experience both rewarding and enjoyable for me.

Many thanks also to Jessica Itxel Vasquez Matias, for providing excellent support in the lab and with the HPLC instrument. Working next to her was a great experience thanks to her exceptional advice and positive attitude.

Lastly, I would like to acknowledge the remaining members of the Giovannitti group. Each of them has supported me in various ways, whether by providing valuable assistance with the project or by contributing to a positive and motivating atmosphere through their kindness and good spirits.

Sebastian Müller, Gothenburg, June 2025

Contents

1
Introduction

Electronic devices are part of our everyday life, including applications such as batteries, solar cells, electrochemical synthesis, and sensors [1][2]. However, the electrodes and active materials used in these settings typically constitute scarce metals such as cobalt and platinum, which limits large-scale production [3]. This is a result of the mining and processing these metals, which is lengthy, requires toxic chemicals and generates copious amounts of waste [4]. Moreover, mining and extraction is moreover often done under unethical working conditions, including child labor [5].

To address this challenge, polymeric organic semiconductors (OSCs), which can be synthesized from earth-abundant elements, are being developed as alternatives [3]. These materials are π-conjugated polymers distinguished by closely aligned energy levels between their highest occupied molecular orbital (HOMO) and lowest unoccupied molecular orbital (LUMO) [6]. In their neutral state, OSCs are typically insulating. Chemical or electrochemical doping introduces excess electrons or electron holes, which can render an OSC conductive [7]. The transport of charges, which is important for achieving high performance in devices, typically occurs within crystalline aggregates, as this is the most energetically favorable pathway. Therefore, connectivity between these aggregates is vital for ensuring good overall conductivity throughout the material [8].

An advantage of polymeric OSCs is their solution processability and compatibility with traditional processing techniques, allowing for inexpensive large-scale manufacturing under mild conditions [9], and facilitating the recycling of devices [10]. Moreover, properties such as solubility, biocompability and microstructure can be tuned through chemical modification of their molecular structure. [6][9][11].

The conductive and mechanical properties of polymeric OSCs depend not only on their molecular structure but also on their microstructural order, which is influenced by their molecular weight (MW) distribution. Polymer chains above a certain length can act as tie chains, connecting different crystalline domains. Such tie chains are crucial for the performance of polymeric OSCs as they facilitate transport of charges between crystallites, something that presents a relatively large energy barrier [8]. However, the MW distribution therefore affects mechanical properties like elastic modulus and phase transition temperatures [12]. The dispersity (Đ), i.e. the width of the MW distribution, is also crucial parameter to consider, as a high Đ can reduce the performance of electronic devices by introducing structural defects that lowers the charge carrier mobility [13]. Optimization of the MW distribution is thus required to yield both favorable conductive and mechanical properties for the target application [8].

A major obstacle in the development of polymeric OSCs is that there are substantial differences in the MW distributions between batches [14]. These batch-to-batch

variations arise from the fact that polymeric OSCs are typically synthesized using step-growth cross-coupling polymerization reactions in which the MW distribution is difficult to control compared to when chain-growth polymerization is used. As a result, there are often significant differences in average MW. Moreover, the batches tend to be highly disperse, meaning they contain a broad mixture of chains with different MWs, where smaller chains can introduce the aforementioned structural defects which lower the performance of devices. Additionally, because the conductive and mechanical properties of an OSC are closely linked to the MW distribution, a wide variety of experimental results can be obtained from different batches of the same polymer. This restricts developing an understanding of a particular polymer as batches are frequently discontinued, as it is difficult to compare the results of studies where different batches are used [15]. Soxhlet extraction is a common method of purifying polymers in which compounds are separated based on their solubility in a specific solvent, although it primarily isolates smaller molecules and oligomers and does not notably lower Đ [16]. Developing methods to narrow Đ, minimize batch-to-batch variations, and obtain similar material from different batches is thus necessary for advancing the field of polymeric OSCs.

Investigating how impurities left from the synthesis of polymeric OSCs affect their electrochemical properties is also important. Particularly, residual Pd impurities from cross-coupling reactions can influence the performance of devices [17]. For instance, one study found that Pd impurities can alter the selectivity of electrosynthetic reactions by acting as a co-catalyst, in this case moving the main product towards water during the electrocatalytic production of hydrogen peroxide in the oxygen reduction reaction (ORR) [3]. In other cases, Pd may catalyze side reactions like the formation of hydrogen peroxide from ambient oxygen, contributing to degradation of devices and being potentially harmful to biological environments [17][18]. There are also indications that the presence of Pd may lower the electronic charge carrier mobility of polymeric OSCs by trapping charges in localized states. Removing side products and metal contaminants is therefore crucial. Again, Soxhlet extraction is a popular method, although it is often insufficient to reduce Pd concentrations to levels that avoid negative effects on device performance and stability [17].

Recent studies have considered preparative high-performance liquid chromatography (HPLC), which is explained in more detail in chapter 2, as a more suitable purification method [19][20][17][21]. Using separation by a type of HPLC known as size exclusion chromatography (SEC), molecules are sorted by size, thereby long polymer chains can be separated from smaller compounds such as Pd, monomers and oligomers [17]. Additionally, the technique enables the separation of polymer batches into fractions with lower dispersity [21]. By recycling eluent back through the same column, its effective length can be increased, facilitating better separation of differently sized components of a sample [19][20][22]. By employing this purification technique to polymeric OSCs, improved purity and lower batch to batch variations can be achieved on a large scale, although its reproducibility and effectiveness across different polymers remain unexplored.

Moreover, SEC can also be used analytically to measure the MW distributions of

polymers. To distinguish this technique from its preparative counterpart, it will be referred to as *analytical GPC* (gel permeation chromatography - a term for size exclusion-based separation) throughout the report. One limitation in using analytical GPC for determination of MW distribution is that the technique is relative, requiring calibration using standards, commonly polystyrene (PS), with well-known MW distributions. The size of a polymer in solution, its hydrodynamic volume, which is the basis for the separation, is largely dependent on extrinsic factors such as temperature, pressure and solvent effects. It is also related to intrinsic factors of the polymer, such as its chemical structure and degree of polymerization, thus the latter can be evaluated using the technique. However, these intrinsic factors also include the rigidity of the polymer backbone, often quantified by its persistence length (l_p). Due to their stiff backbones, polymeric OSCs generally have higher l_p than commonly used calibration standards such as PS, and they are also prone to aggregation [23]. Consequently, even though chains of PS and a polymeric OSC have the same degree of polymerization, differences in l_p and aggregation can lead to significantly different retention times during SEC. Calibration of polymeric OSCs using PS thus leads to an overestimation of the MW, reported by a factor of up to 2.7 for the polymeric OSC *poly(9,9-dioctylfluorene)* (PFO, Figure 1.1b) [24][25]. To better understand how the conductive and mechanical properties of polymeric OSCs are affected by their MW, it is therefore important to investigate how the use of analytical GPC can be improved for a more accurate prediction. A potential way of achieving this is to replace PS with a polymer having more similar stiffness to polymeric OSCs as calibration standard. However, as these polymers are typically highly disperse due to being synthesized using step-growth polymerization, this is not currently possible. This project explores whether preparative HPLC could be implemented to overcome this challenge by isolating fractions with low Đ, which can be compared to PS as calibration standard in future studies.

1.1 Aims

This project aims to explore how preparative HPLC can be applied to polymeric OSCs, and the reproducibility of the technique towards large-scale separation. The latter could be accomplished through employing a highly automated HPLC method with predetermined recycling and collection times. The objective of this thesis is to develop the knowledge required to define these parameters.

Firstly, the method will be developed using *poly(3-hexylthiophene)* (P3HT), shown in Figure 1.1a, which is a well-studied polymeric OSC [26]. P3HT is used as a model polymer to evaluate the reproducibility and performance in isolating fractions with lower Đ compared to the neat sample. Its behavior is however dissimilar to the majority of other polymeric OSCs. For exapmle, P3HT has a significantly lower l_p and can be synthesized using living polymerization rather than step-growth, allowing for more control over the MW distribution and lower Đ [26]. After optimizing the method for P3HT, the objective is therefore to apply the gathered knowledge to separate *poly(9,9-dioctylfluorene)* (PFO, Figure 1.1b), a more typical polymeric OSCs in terms of l_p and Đ, into fractions of narrow Đ and varied MW. The goal is for

these fractions to be used as alternative standards for analytical GPC measurements in future studies. Although it is outside the scope of this project, this would involve measuring the absolute weight-average MW (M_w) of fractions using static light scattering (SLS). As this technique studies the scattering of light, the polymer cannot absorb in the range of the excitation wavelength of the SLS laser, making PFO suitable as due to not absorbing above 450-500 nm in solution [27]. Furthermore, PFO is chosen over P3HT as it has a more similar l_p compared to common polymeric OSCs [28][29].

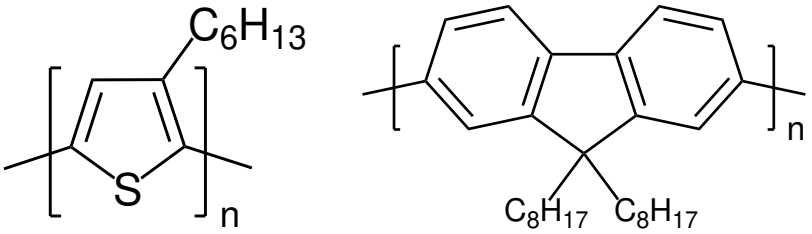

(a) P3HT (b) PFO

Figure 1.1 | Structures of P3HT and PFO. *P3HT (a) is used as a model polymer to develop the HPLC method, which is then applied to PFO (b) to isolate fractions for use as alternative GPC calibration standards.*

1.2 Scope and limitations

To assess the performance of HPLC in isolating fractions with narrow Đ and varied MW, separations are performed with different experimental controls such as collection time intervals and recycling conditions, to study how they affect the MW distributions of the obtained fractions. Reproducibility is tested by applying a given HPLC method to multiple iterations of polymer separation and identifying similarities in fraction distributions.

MW distribution measurements are primarily performed using analytical GPC relative to PS. However, the project also aims to compare different analytical techniques used to determine the MW of polymers. In particular, the focus is on examining the results from MW determination through both GPC and NMR measurements.

The influence of the MW on molecular aggregation behavior is studied through analysis of the UV-vis absorption spectra of polymer thin films and solutions. Thin film measurements are of significance to assess the short-range packing of chains inside solid-state aggregates. In contrast, solution UV-vis measurements give an indication on the degree of intermolecular aggregation in the dissolved state. The latter is conducted on dilute PFO solutions to explore differences in aggregation and conformational behavior of fractions, as similar behavior between fractions is desired for the future SLS measurements.

2

Theory

The following chapter covers the polymers that were used in this work, P3HT and PFO, and the principles of preparative HPLC, analytical GPC and SLS are explained. Moreover, the variations in l_p across different polymers are explored.

2.1 P3HT

P3HT (figure 1.1a) is one of the most extensively studied polymeric OSCs and is commonly used as a model polymer in organic solar cell research. Its popularity arises from its high availability and relatively low cost, made possible by large-scale synthesis using flow chemistry [30], as well as from its well-known properties. Consequently, insights gained from P3HT are often used to predict the behavior of other, higher-performing polymeric OSCs. One study however pointed out that P3HT, despite its popularity, is dissimilar to the majority of these polymers. In comparison, it has a high crystallinity and low glass transition temparture. Additionally, in contrast to other polymeric OSCs which are generally synthesized by step-growth polymerization, P3HT is typically synthesized using a living polymerization process, allowing for better control over the MW distribution. Consequently, batches of P3HT often have lower Đ compared to other polymeric OSCs. For instance, Ossila reports Đ values ranging from 1.75-2.8 [14] for their P3HT batches, whereas PFO batches are more disperse between 2.33-4.23 [31]. These differences suggest that results on P3HT are not directly applicable to other systems, underlining the importance of studying a broader range of polymeric OSCs [26].

A common way of synthesizing P3HT is using a Grignard metathesis polymerization reaction, as illustrated in Figure 2.1. In the first step, 2,5-dibromo-3-hexylthiophene (compound **1**) reacts with a Grignard reagent in an ether solvent, resulting in the formation of two thienyl-Grignard isomers (compounds **2a** and **2b**). With isopropylmagnesium chloride (iPrMgCl) as the Grignard reagent, the ratio of these isomers is roughly 4:1, with **2a** being the major product. In the second step, a nickel-diphosphine catalyst is added to initiate a quasi-living chain-growth polymerization reaction where P3HT is formed. Since the minor isomer (**2b**) is inactive towards the catalyst, only **2a** undergoes polymerization, resulting in a regioregular polymer [30]. By addition of another Grignard reagent in an aqueous solvent, the bromines at the end groups can be substituted with hydrogen [32].

2.2 PFO

PFO (figure 1.1b) belongs to the family of polyfluorenes, which have their main use in optoelectronic devices, such as polymer light emitting diodes (PLEDs), organic solar

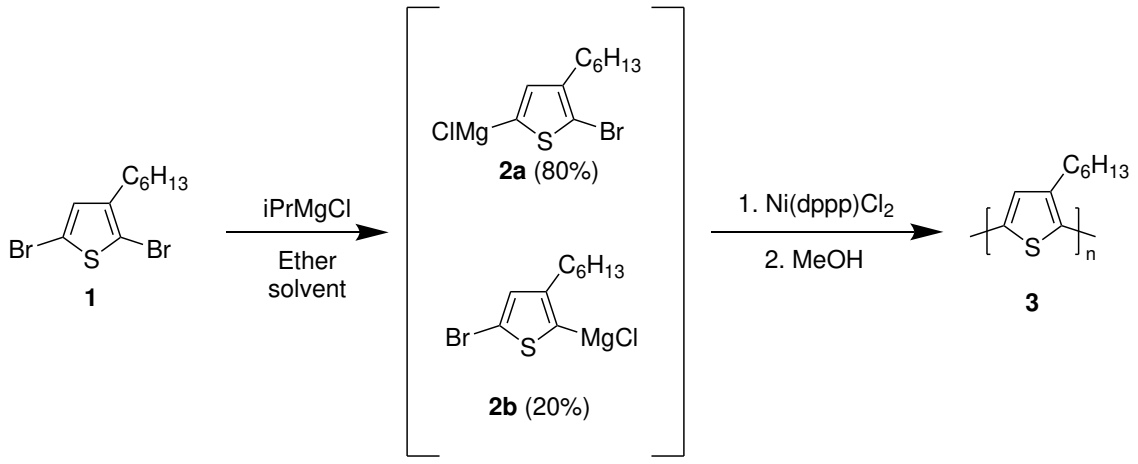

Figure 2.1 | Synthesis of regioregular P3HT by Grignard metathesis.
Reconstructed from [30].

cells and sensors. Advantages of polyfluorenes include their chemical and thermal stability, film-formation properties, and high fluorescence quantum yield. Fluorenes are also easily functionalizatiable at the 2,7 and 9-positions, simplifying synthesis at the 2,7-position and allowing introduction of side chains at the 9-position [33].

2.3 UV-vis characterization of polymers

By studying the optical properties of conjugated polymers, information about molecular aggregation can be obtained. As molecular aggregation in conjugated polymers is strongly driven by π-π interactions perpendicular to the backbone, it affects the electronic structure and, in turn, the spectroscopic properties of the material. The absorption in the UV-vis region, which relates to electronic transitions, can thus provide insight into the aggregation behavior of the polymer. UV-vis measurements are typically performed on polymer solutions and thin films to give information on their aggregation, band gaps and optical transitions in both the solid and dissolved states [34][35].

For thin films of P3HT, the UV-vis spectrum has been reported to show a maximum absorbance at 520 nm with two smaller shoulders at 550 and 610 nm. These shoulders correspond to electronic excitations with 0-1 (550 nm) and 0-0 (610 nm) vibronic transitions. In this context, the 0-0 transition refers to an electronic excitation from the vibrational ground state of the electronic ground state to the vibrational ground state of the excited state, while the 0-1 transition involves excitation from the ground vibrational level of the ground state to the first vibrationally excited level of the electronic excited state. As the 610 nm shoulder is related to a planarization of the polymer chain, caused by aggregation, and becuase the amorphous phase does not absorb at that wavelength, it is useful in comparing the aggregation behavior in different P3HT samples [34][35].

Polyfluorenes mainly show two conformations, an α-phase and a β-phase, in which

the latter consists of more planar chains. UV-vis measurements can give information on these conformations. Solutions of PFO have been reported to show absorption bands at 391 nm, corresponding to the α-phase, while the β-phase is revealed as a smaller peak at 437 nm [36].

2.4 High-performance liquid chromatography

HPLC is a separation technique used to isolate specific chemical compounds from mixtures containing several components. The dissolved sample is injected into a column packed with small adsorbing particles, known as the stationary phase. A solvent, referred to as the mobile phase, is pumped through the system under high pressure. Depending on the affinity for the stationary phase, various components of the sample are separated as they move through the column at different rates. Elution of chemicals from the column is monitored by a detector near the column outlet, generating a chromatogram displaying the detector signal as a function of time [37]. Commonly used types of detectors include UV-vis, refractive index (RI) and mass spectrometry (MS) detectors [38].

While other HPLC separation modes exist, such as those based on polarity, larger molecules like polymers are typically separated based on their size in solution, their hydrodynamic volume. This type of HPLC is commonly referred to as SEC or GPC. In this mode, the stationary phase consists of porous beads. As Figure 2.2 shows smaller molecules remain in the column for longer as they can penetrate the pores of the stationary phase, whereas larger molecules are excluded from the pores and therefore elute more quickly [37]. The Figure displays the separation of a mixture containing three molecules of different sizes, resulting in a chromatogram with three well-separated peaks.

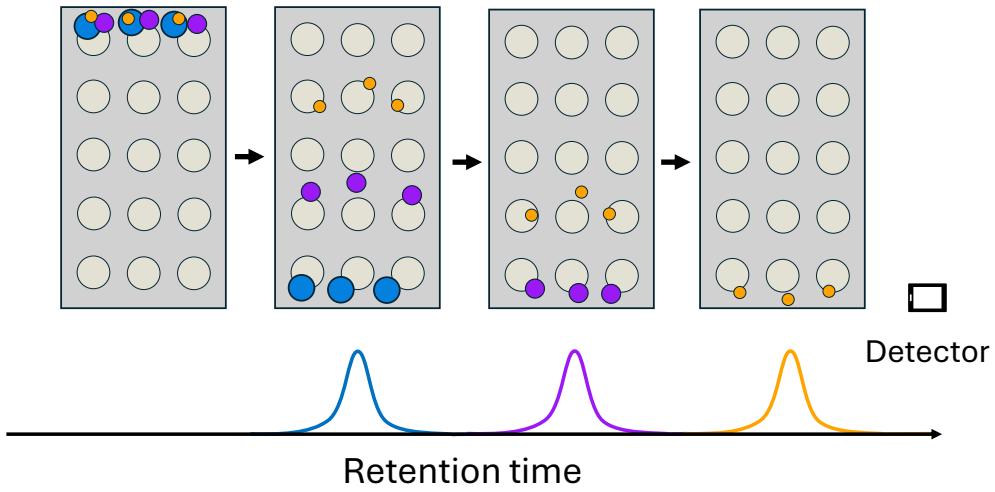

Figure 2.2 | Separation principle of SEC. *Smaller molecules enter the pores of the stationary phase more easily, thus moving slower through the column, while larger molecules elute faster as their size prevents them from infiltrating the pores.*

Increasing the length of the HPLC column can provide a more efficient separation, although this is normally not feasible in practice as column dimensions are not adjustable. To overcome this challenge, material can instead be recycled through the same column, increasing its *effective* length and consequently improving the separation of sample components. Recycling can also reduce the amount of solvent consumed, as no fresh solvent is added to the system during the process. There is however a need to optimize the recycling procedure, as excessive recycling can lead to mixing of small and large molecules. Mixing occurs when larger molecules that have been recycled catch up to smaller molecules from the previous cycle that still remain in the column [22]. Figure 2.3 demonstrates the use of recycling during HPLC. In the first cycle, the three sample components of varying size are poorly separated, resulting in the overlapping of peaks in the chromatogram. Recycling is then performed, slightly improving the separation of the components, although there is still some overlap between the peaks. The sample is thus recycled again, leading to a further improved reparation and three well-resolved peaks in the chromatogram. Recycling a third time however results in mixing of the smallest (orange) and largest (blue) molecules, and an overlap between their respective peaks, annotated by the red arrow.

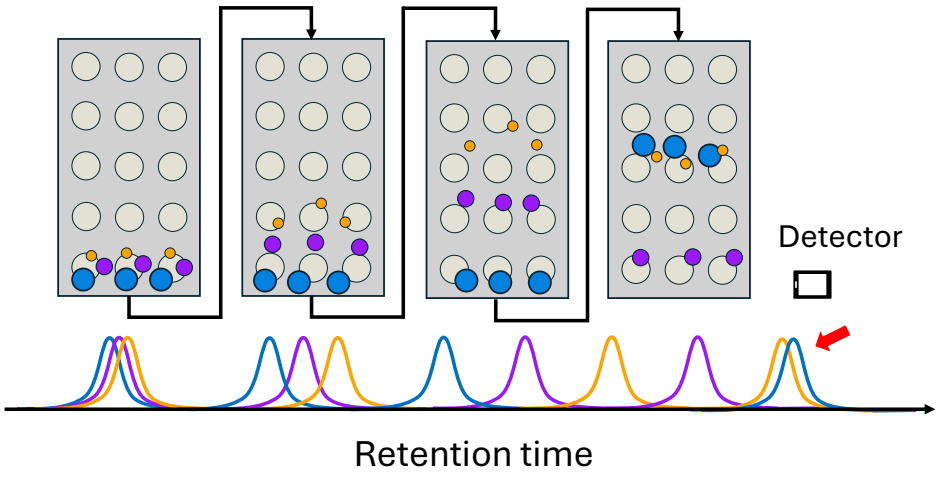

Figure 2.3 | Principle of recycling HPLC. *Recycling can improve the separation during HPLC by increasing the effective column length, but comes with the risk of mixing.*

In addition to optimization of the number of recycles, mixing can be prevented by a method known as *peak shaving*. Peak shaving is performed by removing the trailing portion of the peak of one cycle and the leading portion of the next cycle peak from the recycling loop [22]. In other terms, a fraction of the smallest (slowest) molecules of a cycle and a fraction of the largest (fastest) molecules are removed as these are the most likely to mix.

As mentioned in chapter 1, HPLC can be used for both preparative and analytical purposes (in this report referred to as preparative HPLC and analytical GPC, respectively). Preparative HPLC is used to isolate and purify compounds and normally

uses larger sample volumes, larger columns and higher flow rates than analytical GPC. After passing through the column, the sample can be recovered via a fraction collector. In contrast, analytical GPC is conducted on a smaller scale for the purpose of qualitative and quantitative analysis [39], including the determination of MW distributions of polymers [25].

2.5 Persistence length

The l_p of a polymer is an important parameter to consider when studying its behavior in solution. It reflects the flexibility or stiffness of the polymer backbone, with higher l_p implying a stiffer chain. Structural features such as alternating single and double bonds and six-membered rings can contribute to an increased backbone rigidity. These moieties are common in conjugated polymers, which therefore often exhibit relatively high l_p values [28][40].

Although l_p can vary depending on the solvent and measurement techniques, literature values of PS and a few polymeric OSCs are summarized in Table 2.1. PS is estimated to have an l_p of 1 nm[41], while the polymeric OSCs are reported at several times higher values. Among the polymeric OSCs, P3HT presents a low l_p despite having a higher l_p than PS. PFO falls in the mid-range between 7-9 nm, whereas polymers based on diketopyrrolopyrrole-thiophene (DPP-T) and naphtalenediimide-thiophene-hexyldecyl (NDI-T-H) units show even higher l_p values, with a decrease as more thiophene units are added [28][29].

Table 2.1. Reported persistence lengths for polystyrene and a few polymeric OSCs.

Polymer	l_p **(nm)**
Polystyrene [41]	1
P3HT [28]	2.2-2.9
PFO [28]	7.0-9.0
DPP-T [29]	18.1
DPP-2T [29]	13.8
NDI-T-2HD [29]	21.7
NDI-2T-2HD [29]	17.6

These variations in l_p are what causes inaccuracies in MW distribution measurements of polymeric OSCs when calibrated against PS. Because a higher l_p results in a larger hydrodynamic volume [25][42], a stiffer polymer chain generally moves through the GPC column faster than a more flexible chain of the same MW. Measuring the MW of the stiffer chain relative to the flexible chain, i.e. PS, thus results in an overestimation [25].

2.6 Static light scattering

SLS is a technique that studies the intensity of light scattered by molecules in solution. As Rayleigh theory describes the relationship between this intensity, the

radius of gyration (R_g), and M_w, the two latter parameters can be determined accurately using the technique. This is done by constructing a so-called Zimm plot, in which Kc/R_θ is plotted against $\sin^2(\theta/2)$, where K is the optical constant, c the concentration, θ the measurement angle and R_θ the Rayleigh ratio, which is dependent on the intensity of the scattered light. By performing measurements at different concentrations and linear regression of the data points in the Zimm plot, R_g can be determined as the slope of the line, while M_w is calculated as the y-intercept [43][25].

As SLS studies the light *scattered* by the sample, a requirement for the technique is that the measured compound does not absorb strongly at the wavelength of the SLS laser, as any absorption will reduce the intensity of scattered light by removing photons available to scatter. PFO was chosen for this project partly for this reason - it does not show absorption above 450-500 nm [27], enabling measurements with the available instrument.

3
Methods

3.1 Materials and equipment

Polymers: P3HT (CAS 10934-50-1, Ossila, batch M1010 - 97.3% regioregularity, M_n = 35 240 Da, M_w = 74 000 Da, Đ = 2.1), PFO (CAS 19456-48-5, Ossila, batch M0161A3, M_n = 93 709 Da, M_w = 260 817 Da, Đ = 2.78)

Preparative HPLC: LaboACE LC-7080 Plus (Japan Analytical Industry Co.,Ltd) equipped with a JAIGEL-4HR column and a UV detector. Separations were monitored using JAI Scan software.

Analytical GPC: Agilent 1260 Infinity II (Agilent Technologies, Inc) equipped with three serially connected SDV columns and a UV detector. Calibrated with a ReadyCal Polystyrene PSKITR1-13 kit (Agilent) with 12 data points (M_n from 439 to 2 300 000 Da).

UV-vis spectrometer: Cary 60 (Agilent Technologies, Inc).

3.2 Preparative HPLC

Preparative HPLC was used to separate commercial polymer samples into fractions for further analysis. There are two modes in which the HPLC can be operated - manual and automatic. In manual mode, the user controls when to collect fractions or recycle material through the column. In automatic mode, the instrument instead applies a predetermined recycling and fraction collection scheme that is defined by the user.

Polymers were dissolved in EtOH stabilized chloroform with 0.5% HPLC-grade triethylamine (TEA) to a concentration ranging from 12-25 mg/ml depending on the availability of starting material and the solubility of the polymer. Solutions were prepared in dried glassware under inert atmosphere using Schlenk technique. To ensure full dissolution of the sample, solutions were heated to 40 °C under stirring. After cooling to room temperature, solutions were filtered with a 0.45 μm PVDF or glass fiber syringe filter to prevent dust or other particles from entering the column.

Separations were performed using EtOH stabilized chloroform with 0.5% TEA as mobile phase, with a pump flow rate of 40 ml/min. The pressure was between 3-4 MPa throughout the separations. Fractions were collected in 2-minute intervals for all separations as this would provide a reasonable number of fractions and for fair comparison between the various separations. Unless otherwise stated, the UV detector was set to 350, 400, 550 and 700 nm.

Following the separation, solvent was evaporated from each fraction in a rotary evaporator. Fractions were then redissolved in a minimal amount of chloroform under heating (40-45 °C). P3HT fractions were thereafter precipitated in 25-75 ml methanol - where a larger amount of polymer was expected, more methanol was used. The precipitate was then filtered with vacuum. To save time, PFO fractions were instead solidified directly by evaporation instead of precipitation and filtration. After this step, samples were vacuum dried for at least 2 hours using Schlenk technique.

3.3 Analytical GPC

Analytical GPC was used to determine the MW distributions of fractions obtained from the HPLC separations. The technique was also used prior to the separations to give an understanding of the MW distributions of the samples that can be utilized during the HPLC. The analytical GPC was calibrated by running a series of PS standards with known MW distributions, which are used to calibrate elution time with molar mass in Da. From the measured MW distributions, the number-average MW (M_n), M_w and Đ (defined as M_n/M_w) were extracted.

Polymer solutions were prepared in HPLC-grade chloroform at 1 mg/ml, except in one case where the concentration was 0.5 mg/ml as the amount of polymer was insufficient to run it at a higher concentration. Solutions were heated at 40-45 °C until they were fully dissolved. Similarly to the HPLC samples, the solutions for GPC were filtered with a 0.45 μm glass fiber filter before the analysis.

Analytical GPC measurements were carried out using chloroform as the mobile phase with a flow rate of 1.0 ml/min at 35 °C. MW distribution data was extracted with the UV detector set to 254 nm.

3.4 UV-vis measurements

Thin films for UV-vis measurements were coated on glass slides that had been cleaned using an ultrasound bath in 1) soapy water 2) acetone and 3) isopropanol for 15 minutes each. Polymer solutions were prepared in chloroform at 10 mg/ml and heated at 45 °C until they were fully dissolved. Films were spin coated at 2000 rpm for 60 s using 175-200 μl polymer solution.

Polymer solutions for UV-vis measurements were prepared at 0.017 mg/ml in EtOH stabilized chloroform.

The UV-vis measurements were done using a scan rate of 300 nm/s. 3 The transmittance of samples was measured and converted manually to absorbance.

3.5 Determining DP_n for P3HT using NMR

NMR measurements were performed for neat P3HT and some P3HT fractions at 70 °C in trichloroethylene-d (TCE-d) with a polymer concentration of 10 mg/ml.

Samples were prepared by dissolving 5 mg in 0.5 ml TCE-d under heating with a heat gun.

The average degree of polymerization (DP_n) was determined for using ^{1}H NMR according to [32]. This was done by analysis of the protons h, at the end groups, and b, in the main chain, as in Figure 3.1.

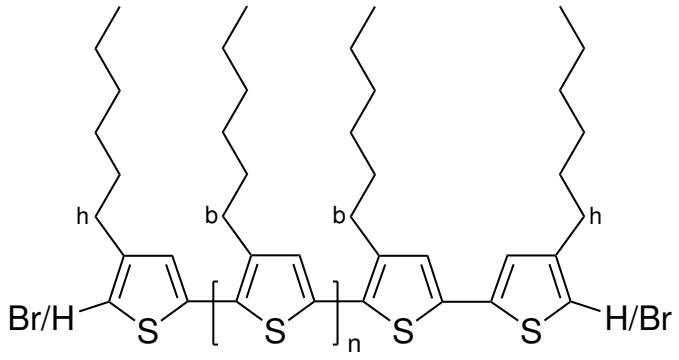

Figure 3.1 | Determining DP_n for P3HT using NMR. *The set of protons in the end groups (h) appear at a lower chemical shift than the corresponding main chain protons (b). The relative ratio of the peak integrals can thus be used to estimate DP_n.*

In the article, b appeared at a chemical shift of around 2.8 ppm, while h demonstrated a slightly lower shift at 2.6 ppm. If the side chains contain hydrogen on both sides at the position adjacent to the sulfur (H/H), h becomes a single triplet, whereas if they contain bromine on one side and hydrogen on the other (H/Br), the peak splits into two triplets. Nevertheless, by taking the relative ratio of the integrals of the b and h peaks, DP_n can be calculated. At position h there are 4 protons in total ($n_a = 4$). At position b there are 2 protons for each repeating unit, meaning 2 times DP_n protons in total ($n_b = 2 * DP_n$). The ratio between the integrals I_b/I_h is equivalent to the ratio between the total number of b-protons to the number of h-protons, hence the relationship in equation 3.1 applies.

$$\frac{I_b}{I_h} = \frac{n_b}{n_h} = \frac{2 * DP_n}{4} = \frac{DP_n}{2} \tag{3.1}$$

Solving for DP_n gives $DP_n = \frac{2I_b}{I_h}$. Setting I_h to 2 in the NMR software gives DP_n as the relative integral of the b-peak. From DP_n, using the monomer mass for P3HT (166.282 g/mol), the number-average MW (M_n) was also determined.

4

Results

For P3HT, a preparative recycling HPLC separation protocol was previously developed by M.Denis [20]. Initially, the reproducibility of the HPLC method was tried by repeating the protocol in two iterations, running the HPLC in automatic mode with the same event times for both. In addition to MW distribution measurements of the obtained fractions, UV-vis and NMR measurements and were performed on fractions from the second iteration, to study their solid-state aggregation behavior through their absorption spectra and determine their MW via NMR. Moreover, the effect of recycling was studied by separating P3HT again, this time without recycling, and comparing the MW distributions of the obtained fractions.

The collected fractions from these separations contained polymer mostly above the MW where P3HT chains start to entangle. Below this threshold is where the largest variations in material properties are expected [44]. Therefore, the collected peak shaving regions from the first two separations of P3HT were separated, with the main goal of isolating unmixed fractions of low MW polymer. This was done twice with varying recycling protocols.

After separation methods were developed for P3HT as mentioned, separations of PFO were performed with the objective of producing fractions that could be investigated as novel calibration standards for analytical GPC. Also this was done in two attempts with different recycling procedures. Additionally, solutions of these fractions were measured with UV-vis to study molecular aggregation in their dissolved state.

Aside from the initial separation of neat P3HT, where a protocol was alredy developed prior to this project, new separation methods were developed and optimized. This was done by separating polymers in manual HPLC while trying various recycling and peak shaving procedures. After each separation, the MW distributions of fractions were measured with analytical GPC to investigate their Đ and potential mixing. If required, separations of the same polymer where thereafter repeated while adjusting the recycling and peak shaving protocol.

This chapter covers the results that were acquired through the aforementioned separations and characterizations of the obtained polymer fractions.

4.1 Separation of neat P3HT

Table 4.1, summarizes the MW distribution of the neat P3HT batch, comparing data measured with the analytical GPC to supplier-provided data. Although the supplier does not specify the measurement technique used, the results show clear similarities.

Table 4.1. MW distribution data for neat P3HT.

	M_n (kDa)	M_w (kDa)	Đ
Supplier [14]	35	74	2.1
GPC	34	77	2.29

To test the large-scale reproducibility of the HPLC method, P3HT was separated in two repeat iterations (P3HT Neat iteration 1 and P3HT Neat iteration 2). These separations were performed using the previously developed sample preparation and automatic injection protocol, using roughly 600 mg P3HT with a polymer concentration of 25 mg/ml. Due to the large volume of sample and the limited injection volume allowed by the instrument, the separation was performed with three repeated injections, each with a volume of 7 ml. Figure 4.1 presents the chromatograms of the first injections for the two iterations. Detailed time intervals for recycling and fraction collection are provided in Table A.1. The full chromatograms showing all three repeat injections can be found in Figure B.1.

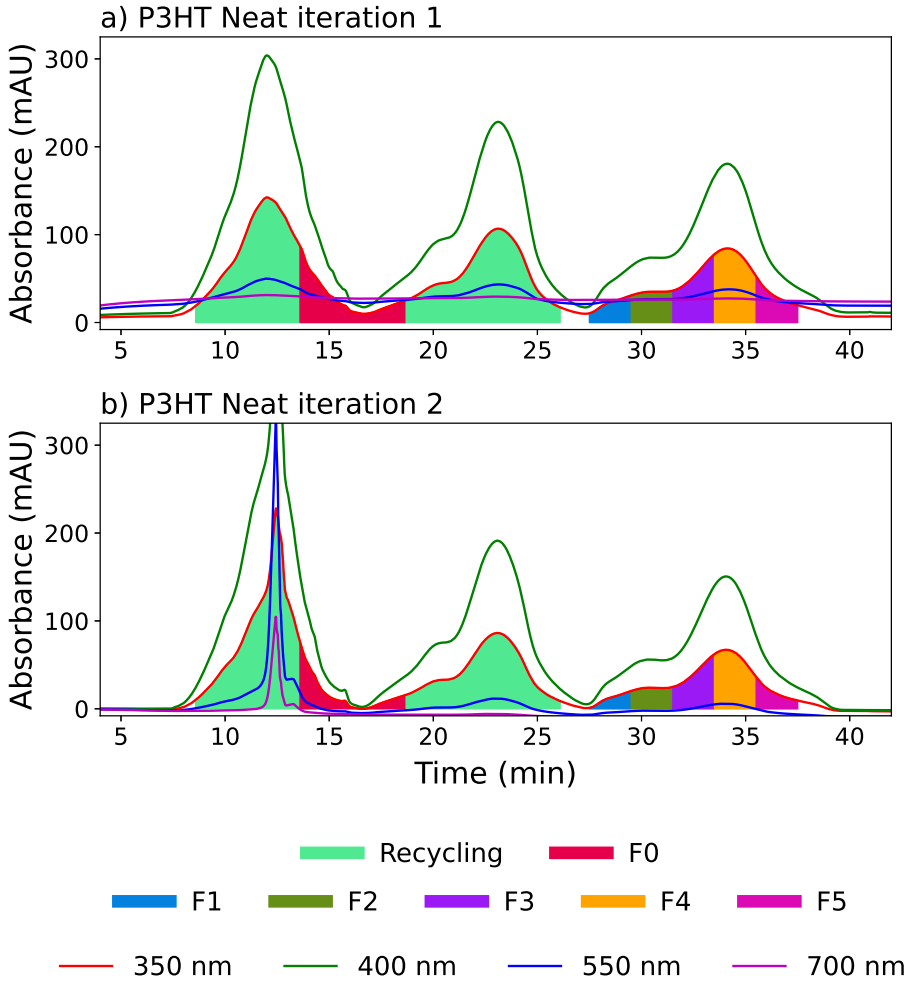

Figure 4.1 | Separation of neat P3HT. *Chromatograms from the a) first and b) second separations of neat P3HT, using the previously developed separation protocol.*

For both of these separations, the sample was firstly recycled immediately after detection between 8 and 14 minutes (shown in light green, Figure 4.1), followed by collection of the smallest chains and the largest chains in the second column pass (peak shaving). The latter is referred to as 'Fraction 0' (F0) and is shown in red in Figure 4.1a and b. F0 is collected to prevent mixing with the next cycle. The sample was then recycled once more, whereafter five fractions (F1-F5 in Figure 4.1) were collected in 2-minute intervals during the third cycle, shown by the filled areas in various colors beneath the third peaks of each set. A lower fraction number means a shorter retention time, which is correlated to a higher hydrodynamic volume of polymer chains in the fraction. Fractions with higher numbers have longer retention times and thus contain polymers of lower hydrodynamic volume.

The two chromatograms exhibit clear similarities in both peak shapes and intensities, which could be an initial indication of reproducibility between the two separations. In the first peak of each repeated injection, the intensities, which relate to the concentration of the sample, are consistently around 250-300 mAU at 400 nm, with a slightly lower intensity at the third injection of P3HT Neat iteration 1 (Figure B.1a). An exception is the first peak of P3HT Neat iteration 2, in which a distinct spike reaching close to 450 mAU at 400 nm is observed. Notably, this spike is also present at 700 nm, where P3HT normally does not absorb. The spike is also only present in the first repeat injection, see Figure B.1. Likely, this is an artifact caused by a fault in the injection of the sample or something else during the run. A possible explanation is that air entered the column, forming bubbles that caused the increase in absorbance.

In Figure 4.2, the MW distributions of the fractions obtained from P3HT Neat iteration 1 (solid lines) and 2 (dashed lines) are compared. The MW distrubition of the neat polymer (dotted) is also included. Despite efforts to ensure consistent concentrations for analysis, the distributions are normalized to disregard the influence of minor concentration differences. The MW distributions of fractions from the first iteration are closely reproduced in the second iteration, except for a small shoulder in F4 of P3HT Neat iteration 1 (orange solid line in Figure 4.2). Shoulders are also seen in F1 and F2 for both iterations around 50 kDa. Most likely, these shoulders result from mixing due to recycling. Nevertheless, the similarities in the distributions clearly show that the fractions are nearly identical in terms of their MW distributions. Moreover, Compared to the neat sample, the fraction distributions appear more narrow. Particularly at the base of the peaks, the neat sample never fully approaches zero on the y-axis, while the fractions approach zero much more quickly.

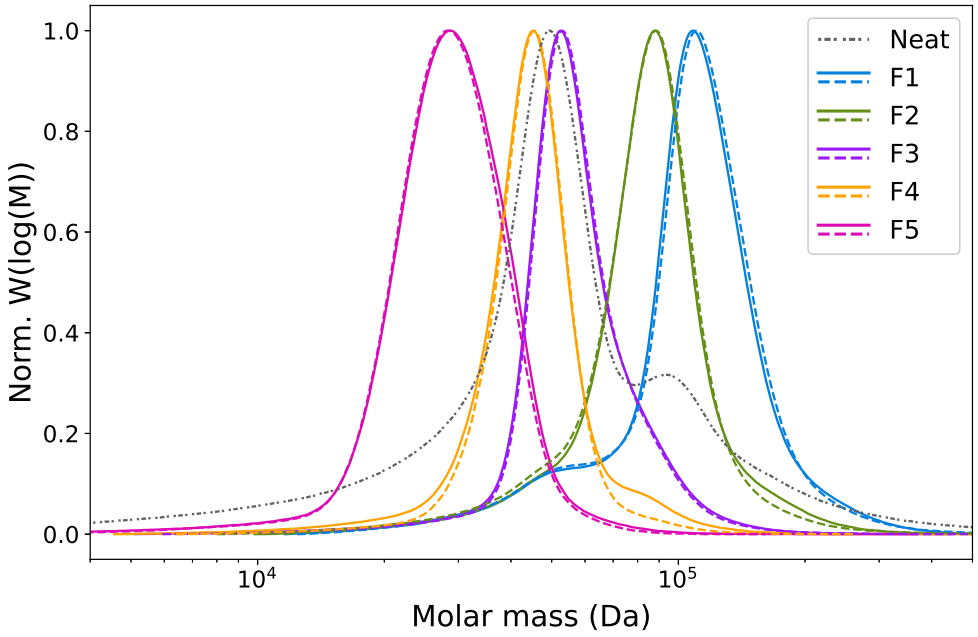

Figure 4.2 | Normalized MW distributions of fractions isolated from neat P3HT. *The obtained fractions from P3HT Neat iteration 1 (solid) and 2 (dashed) exhibit similar MW distributions with less dispersity than the neat polymer (dotted).*

M_n, M_w and Đ values, determined by the analytical GPC software from the MW distributions in Figure 4.2, together with the yields for each fraction are summarized in Table 4.2. As expected, F1-F5 are ordered from highest to lowest M_n and M_w for both separations, with F1 having the highest and F5 the lowest average MWs. All fractions have relatively low dispersities, with the highest being F1 at 1.23 for both separations, followed by F2. This is a result of the slight mixing which causes shoulders to appear in their distributions, as explained earlier. Moreover, the largest difference in Đ values are for F4, with an increase by 0.05 for P3HT Neat iteration 1, explained by the shoulder that was not observed in P3HT Neat iteration 2. Including F0, the total yields were 74% (597.7 mg starting material) and 79% (599.0 mg starting material) for the first and second separations, respectively. Among the individual fractions (not including F0), F3 and F4 showed a significantly higher yield than the other fractions, ranging from 16-24%. Moreover, the two iterations resulted in closely similar yields for all corresponding fractions.

Table 4.2. MW distribution data and yields for the separations of neat P3HT.

	P3HT Neat iteration 1				P3HT Neat iteration 2			
	M_n (kDa)	M_w (kDa)	Đ	Yield (%)	M_n (kDa)	M_w (kDa)	Đ	Yield (%)
F0	-	-	-	15	-	-	-	15
F1	93	114	1.23	5	94	115	1.23	5
F2	77	90	1.17	9	74	88	1.19	10
F3	53	60	1.13	17	54	60	1.12	16
F4	42	47	1.13	21	43	46	1.08	24
F5	27	30	1.15	7	26	30	1.13	8

For the P3HT Neat iteration 2 fractions, UV-vis measurements were performed on thin films. Figure 4.3 shows the normalized absorbance spectrum for the measured fractions. As reported in literature, the spectrum features two shoulders at 550 and 610 nm, corresponding to different electronic transitions, and a maximum absorbance at 520. For F1, F4 and F5, there is also a slight red-shift which is apparent near 650 nm. Inspecting the shoulder at 610 nm, there are no major differences, although it is generally slightly more pronounced with decreasing MW, implying that shorter chains resulted in a higher degree of molecular aggregation. An exception is the highest MW fraction (F1), for which the shoulder is more pronounced, being mostly overlapped with F4.

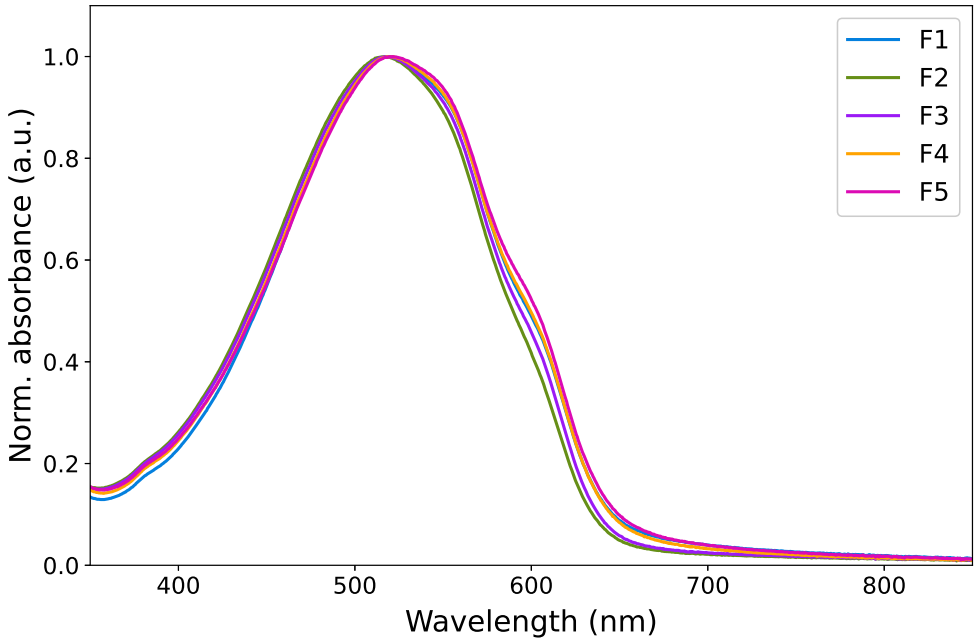

Figure 4.3 | Normalized UV-vis spectra for P3HT films. *Measurements were performed on fractions from P3HT Neat iteration 2. The shoulder at 610 is generally more pronounced with decreasing MW, with the exception of F1.*

4.1.1 Determining DP_n through NMR

NMR measurements were performed on P3HT Neat iteration 2 fractions and the neat polymer. The goal was to determine DP_n and M_n to compare NMR to analytical GPC. Figure 4.4 shows the NMR spectrum of neat P3HT, zoomed in to the peaks that were used for this analysis. The left peak at 3.3 ppm corresponds to the b-protons in the main chain while the right peak at 3.1 ppm results from the h-protons in the end groups, as described in section 3.5. The integration range that was used for the analysis is shown by the horizontal green lines below the peaks. NMR spectra for the other measured samples can be found in Appendix C.

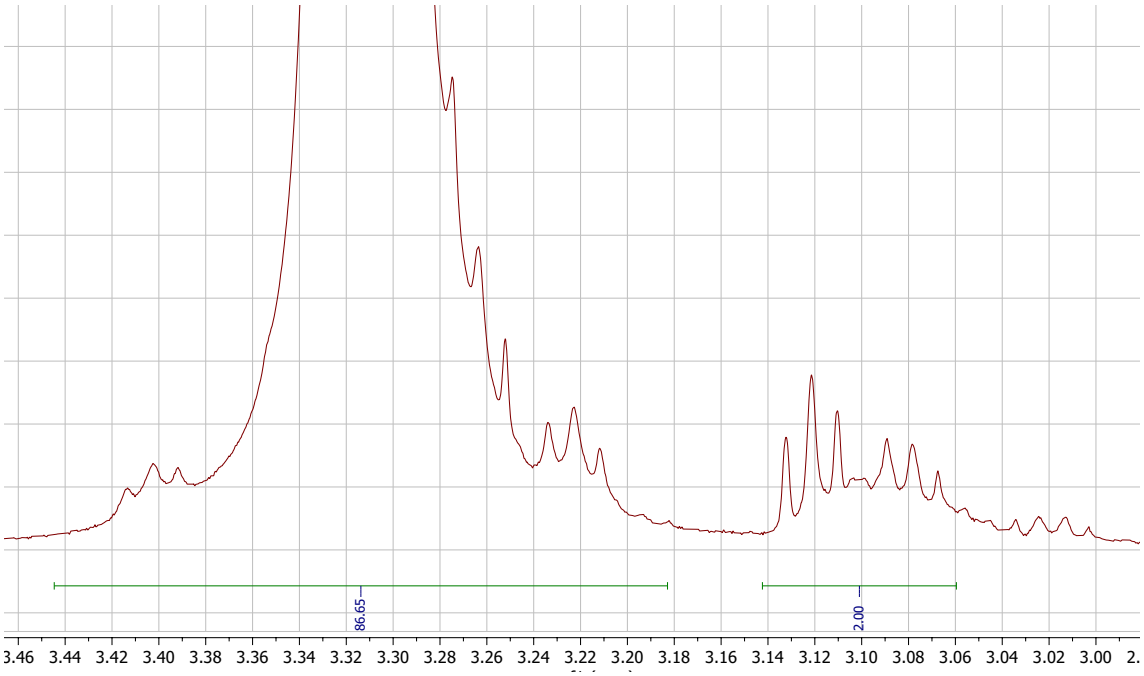

Figure 4.4 | Zoomed-in NMR spectra of neat P3HT. *The larger peak at 3.3 ppm corresponds to the main chain protons while the smaller peaks around 3.1 ppm relates to protons in the end groups.*

Compared to what was reported in [32], the peaks are at a slightly higher chemical shift, although this may result from the fact that a different solvent was used. For the right peak, the splitting is somewhat difficult to distinguish, although it is seemingly split into two triplets, indicating that at least some chains contain H/Br end groups.

In Table 4.3, the determined DP_n and M_n values from NMR and GPC are compared. For the fractions of P3HT Neat iteration 2, the trend is the same when both techniques are used - the values are in order of the fraction number, where F1 has the highest and F5 the lowest DP_n and M_n. However, the GPC values are significantly higher in all cases. The calculated values of corresponding fractions using the two methods were generally closer with decreasing chain length, with GPC values being 2.6 times higher for F5 while they are more than 5 times higher for F1 and F2.

Table 4.3. Degree of polymerization and number-average molecular weights for P3HT Neat iteration 2 fractions, determined using both GPC and NMR.

	$DP_{n,NMR}$	$DP_{n,GPC}$	$M_{n,NMR}$ (kDa)	$M_{n,GPC}$ (kDa)
Neat	87	204	14	34
F1	106	565	18	94
F2	82	445	14	74
F3	79	325	13	54
F4	75	259	12	43
F5	59	156	10	26

4.1.2 Separation of neat P3HT without recycling

With the goal of investigating how recycling affects the separation of P3HT, an additional separation (P3HT Neat C1, where the number following C refers to the cycle number at which fractions were collected) was carried out without recycling. Here, the polymer concentration was the same as the previous separations at 25 mg/ml. Figure 4.5 shows the chromatogram from this separation. The HPLC was run in automatic mode and fractions were collected in 2-minute intervals starting from the same time as the first recycling interval in the two previous separations. Four fractions were collected from this run. Similarly to P3HT Neat 2 (Figure 4.1b), a spike was observed in the chromatogram around 13 min, again suggesting that an issue occurred in the injection or with something else during the run. Notably, a considerate amount of sample remained uninjected, supporting the claim that an error took place in the injection step.

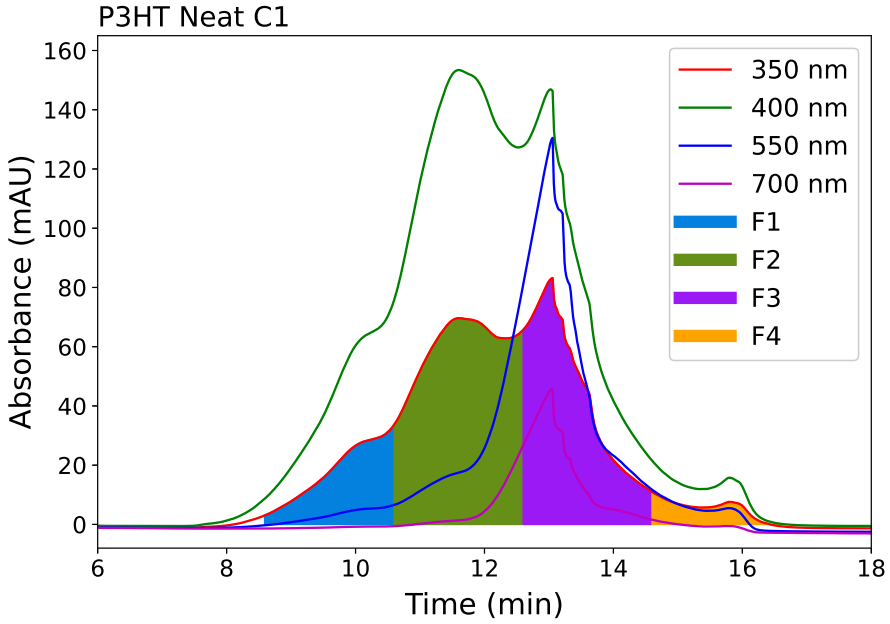

Figure 4.5 | Chromatogram from separation of neat P3HT without recycling.

Figure 4.6 shows the measured MW distributions of F1, F2 and F3. F4 could not be measured due to the low sample amount. Compared to the distributions of the previous separations of P3HT in Figure 4.2, the peaks are much broader here - note that the x-axis is zoomed out compared to the previous graph. This particularly applies to F3, which features a shoulder in its upper MW range that almost completely merges with F2.

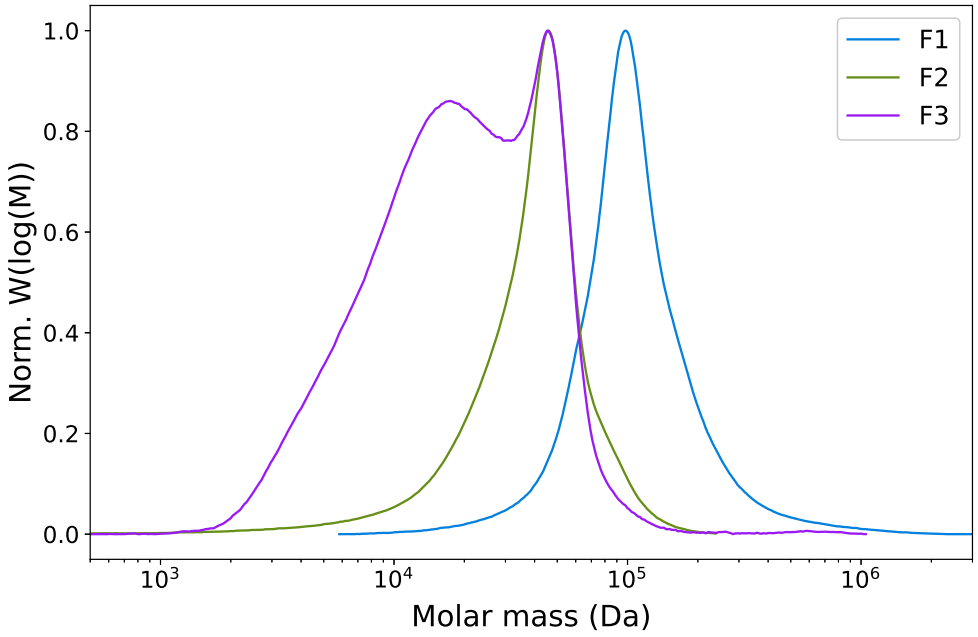

Figure 4.6 | Normalized MW distributions of fractions from P3HT Neat C1. *Separation without recycling yielded broader distributions.*

Table 4.4 shows the MW distribution data for the measured fractions. Although Đ was higher for all fractions compared to P3HT Neat iteration 1 and 2, it was still lowered compared to the neat polymer (Đ=2.29, Table 4.2), with the most disperse being F3 at 2.08. Because of the faulty injection of the sample, the yields were overall low, with a total of 30.4% recovered. The individual yield for F2 was considerably higher compared to the other fractions, at 20.7%, with the second to highest being F1 at 5.7%.

Table 4.4. MW distribution data and yields for P3HT Neat C1 fractions.

	M_n (kDa)	M_w (kDa)	Đ	Yield (%)
Neat	35	77	2.29	-
F1	89	130	1.46	5.7
F2	25	43	1.76	20.7
F3	13	27	2.08	3.8
F4	-	-	-	0.2

4.2 Separation of F0

As F0 contained the both the highest and lowest chain lengths from the neat polymer sample, further separation was carried out in an attempt to access a wider range of MW P3HT samples. Two attempts were carried out with different recycling procedures - in the first attempt (P3HT F0 C3, 4.7a) the sample was recycled twice and fractions were collected during the third cycle. In the second attempt (P3HT

F0 C2, 4.7b), recycling was performed once and fractions were instead collected during the second cycle. The chromatograms from these two attempts are shown in Figure 4.7, with the recycling and collection protocol found in Table A.3 and A.4, respectively.

In P3HT F0 C3 (Figure 4.7a), the sample concentration was lowered to 15 mg/ml as the amount of starting material was lower compared to the separation of the neat polymer. During the separation, sample was recycled through the column twice, followed by peak shaving between 29 and 31.5 minutes, as shown by the non-colored area in Figure 4.7 between the second and third cycles. Six fractions were thereafter collected during the third cycle. As can be seen at around 30 minutes in the chromatogram, the peaks from the second and third cycle appear to overlap, suggesting that mixing may have occurred in the high MW fractions. As is revealed from the MW distributions in Figure 4.8a, this is clearly the case for F2, F3 and F4, which all demonstrate distinct smaller peaks above 100 kDa. This is further supported by the high Đ for these fractions shown in Table 4.5, where the data for both attempts are presented. Surprisingly, F1 does not appear to be mixed and has a very low Đ of 1.04.

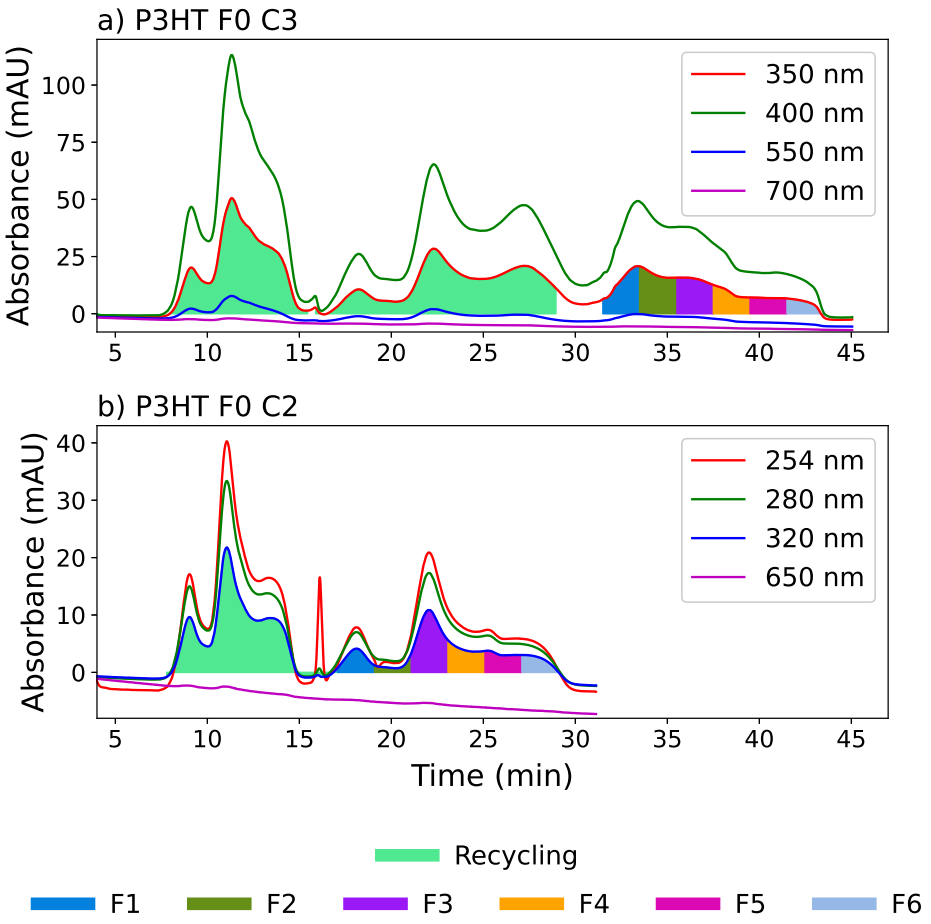

Figure 4.7 | Separation of F0. *Chromatograms from the two separations of F0, with a) collection during the third cycle, and b) during the second cycle.*

Because fractions from P3HT F0 C3 showed mixed MW distributions, which was assumed to be due to excessive recycling, the second attempt (P3HT F0 C2, Figure 4.7b) was performed by collecting fractions during the second cycle instead of the third. Due to the even lower availability of starting material compared to the first separation, it was necessary to lower the concentration to 12 mg/ml. Moreover, the detector was set to other wavelengths compared to the rest of the separations. A noticeable baseline drift is also present, as indicated by the decreasing absorbance at 650 nm. Whilst there are similarities in peak shapes between the two runs, these combined factors complicate comparison of the chromatograms.

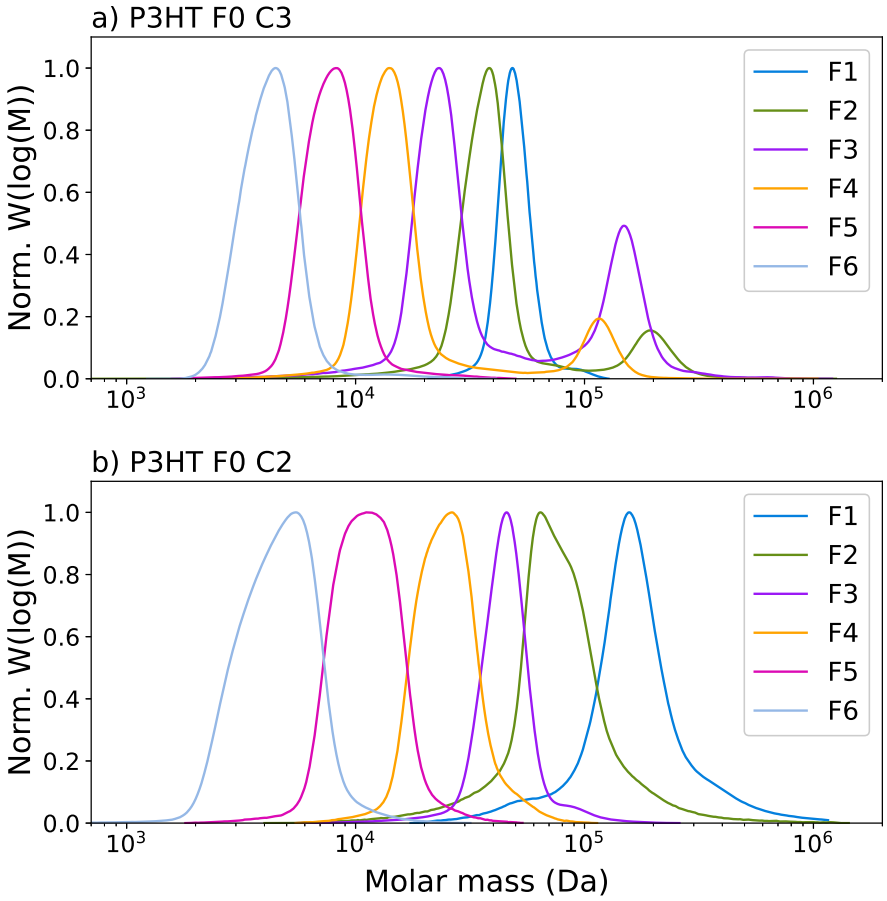

Figure 4.8 | Normalized MW distributions of fractions from the separation of F0. *a) Collection during the third cycle resulted in mixed MW distributions for F2-F4. b) Collecting during the second cycle yielded slightly broader but unmixed distributions.*

Compared to P3HT F0 C3, the MW distributions of P3HT F0 C2 (Figure 4.8b) generally exhibit slightly broader peaks, suggesting an increase in dispersity. No smaller peaks are however observed in addition to the main peaks, so no major mixing was suspected at first glance. For F1 and F2, however, the peaks contain slight shoulders around 40 and 100 kDa, respectively. In addition, the peaks are relatively wide at their bases, indicating potential mixing for these fractions.

The data in Table 4.5 shows M_n, M_w, Đ and yields for the P3HT F0 C3 and 2 fractions. Collection during the third cycle in P3HT F0 C3 resulted in Đ ranging from 1.04-1.10 for F1, F5 and F5, whereas F2, F3 and F4 had higher Đ of 1.63-2.25, explained by the smaller peaks in Figure 4.8b caused by mixing. Collection during the second cycle in P3HT F0 C2 rendered Đ of 1.10-1.34, somewhat higher than the unmixed fractions. Yet, these are relatively low values compared to the neat polymer. The four lowest MW fractions all exhibit excellent Đ below 1.2, while F1 and F2 are slightly more disperse, likely connected to their slightly mixed MW distributions as explained. The data moreover confirms that further separation of F0 enabled the acquisition of low MW polymer fractions, with the lowest two fractions of P3HT F0 C2 having M_n of 11 and 4 kDa, respectively. Also some high MW (M_n = 140 kDa) was obtained in F1. In terms of yield, P3HT F0 C3 gave a total yield of 53 % from 88.9 mg of starting material, with F2 and F3 showing the highest individual yields. P3HT F0 C2 resulted in a total yield of 49 % from approximately 60 mg of starting material, with the highest individual yield observed for F3.

Table 4.5. MW distribution data and yields for the separations of F0.

	P3HT F0 C3				P3HT F0 C2			
	M_n (kDa)	M_w (kDa)	Đ	Yield (%)	M_n (kDa)	M_w (kDa)	Đ	Yield (%)
F1	49	51	1.04	7	140	188	1.34	7
F2	38	61	1.63	12	66	90	1.37	4
F3	29	64	2.25	12	43	47	1.10	18
F4	16	28	1.81	6	24	27	1.11	8
F5	7.6	8.3	1.09	9	11	12	1.12	6
F6	4.1	4.5	1.10	7	4.2	4.9	1.17	6

4.3 Separation of PFO

The MW distribution of the neat PFO sample, measured with the analytical GPC, is shown in Figure 4.9. A small peak in the distribution can be seen at M_n = 9500 kDa.

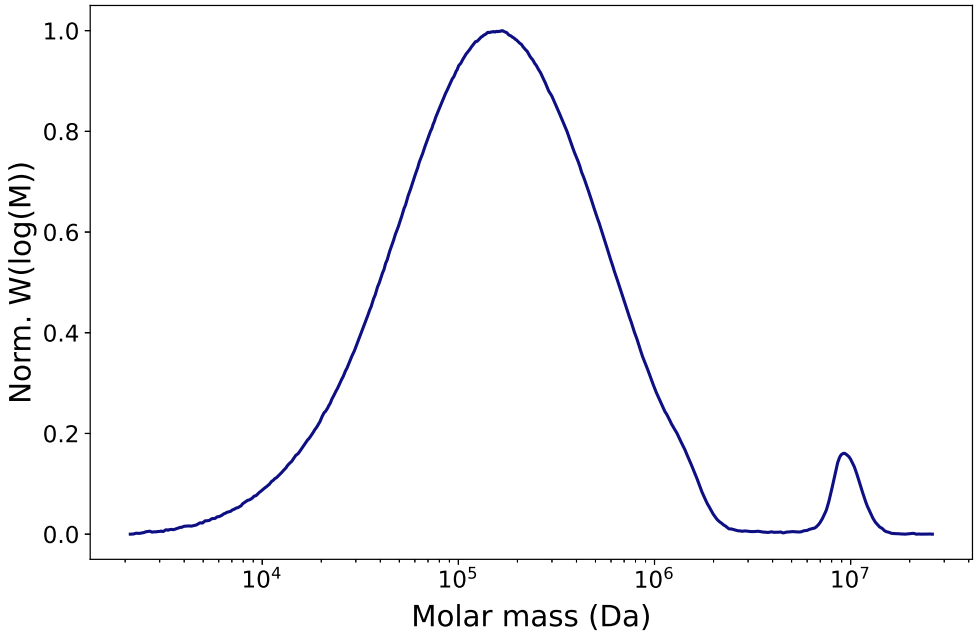

Figure 4.9 | Normalized MW distribution of neat PFO. *A small peak was observed around 10^7 Da in addition to the main distribution peak.*

In Table 4.6, analytical GPC data for the larger main peak is compared to the data provided by the supplier. When considering just the main peak, the GPC data agrees somewhat poorly with the supplier data - M_w are similar at around 260 kDa while M_n is higher at 94 kDa for the supplier data compared to 74 kDa measured with the GPC. This resulted in a higher Đ for the GPC measurement at 3.63 compared to the supplier data at 2.78. This error could result from the use of different instruments, solvents and concentrations, and is likely within the margin of error of the system. Comparing the measured main peak to the distribution of neat P3HT, which was measured at 2.29 (Table 4.2), PFO was more disperse. This means that more fractions would likely need to be collected for PFO to achieve as low Đ as for the P3HT fractions.

Table 4.6. MW distribution data for neat PFO.

	M_n (kDa)	M_w (kDa)	Đ
Supplier [31]	94	261	2.78
GPC (main peak)	72	262	3.63

With the developed knowledge of how HPLC could be used to lower the dispersity for P3HT, the goal of separating PFO was to isolate fractions that could be tried and compared to PS as calibration standards for analytical GPC measurements. For all PFO separations, the sample concentration was lowered to 12.5 mg/ml compared to the separations of neat P3HT, as PFO showed a lower solubility compared to P3HT. Firstly, a test run was done to get an understanding of how the polymer behaved in the HPLC. Although no fractions were collected in this run, the chromatogram is shown in Figure 4.10. The high MW polymers in the smaller peak from the MW distribution in Figure 4.9 were anticipated to elute first. However, this peak did not appear separately from the main peak in the HPLC chromatogram. Potentially, it could be included in the main peak as the small shoulder seen just before 8 minutes.

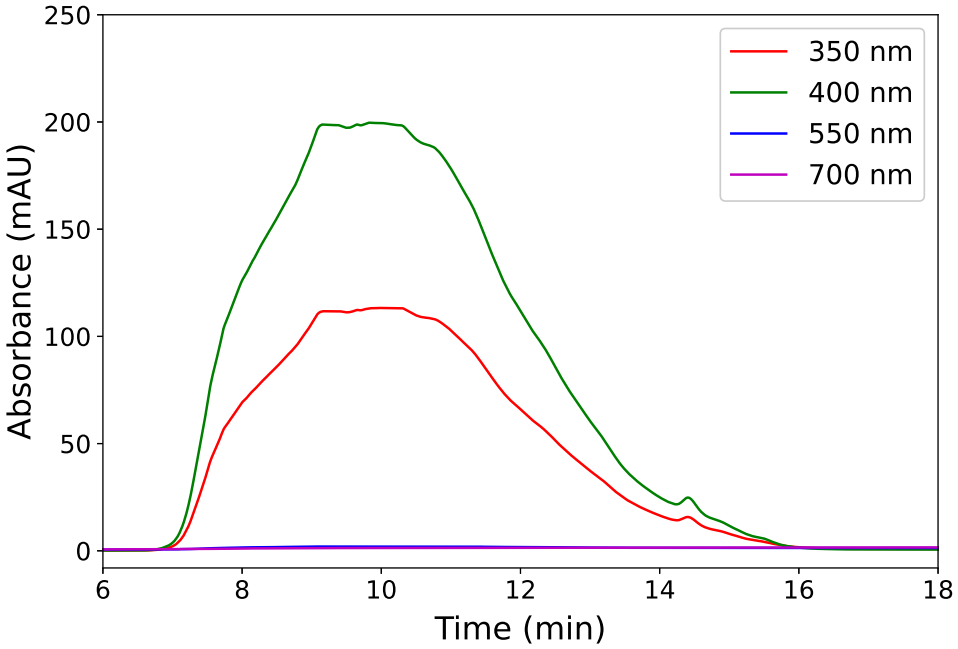

Figure 4.10 | Chromatogram from PFO test run.

Being more familiar with the HPLC chromatogram, the next separation (PFO C2, Figure 4.11a) was carried out. As the chromatogram in the test run (Figure 4.10) showed that PFO elutes between 7 and 16 minutes, recycling was performed to enable collection of more than five fractions while maintaining a 2-minute collection interval. Moreover, because the test chromatogram exhibited a fairly long tail after 13-14 minutes, peak shaving was done by collecting an F0 around this point in an attempt to minimize mixing of the subsequent fractions. A slight overlap can be seen between the first and second cycles in Figure 4.11a), highlighting the importance of this initial collection as mixing would likely occur otherwise. Six fractions were thereafter collected during the second cycle.

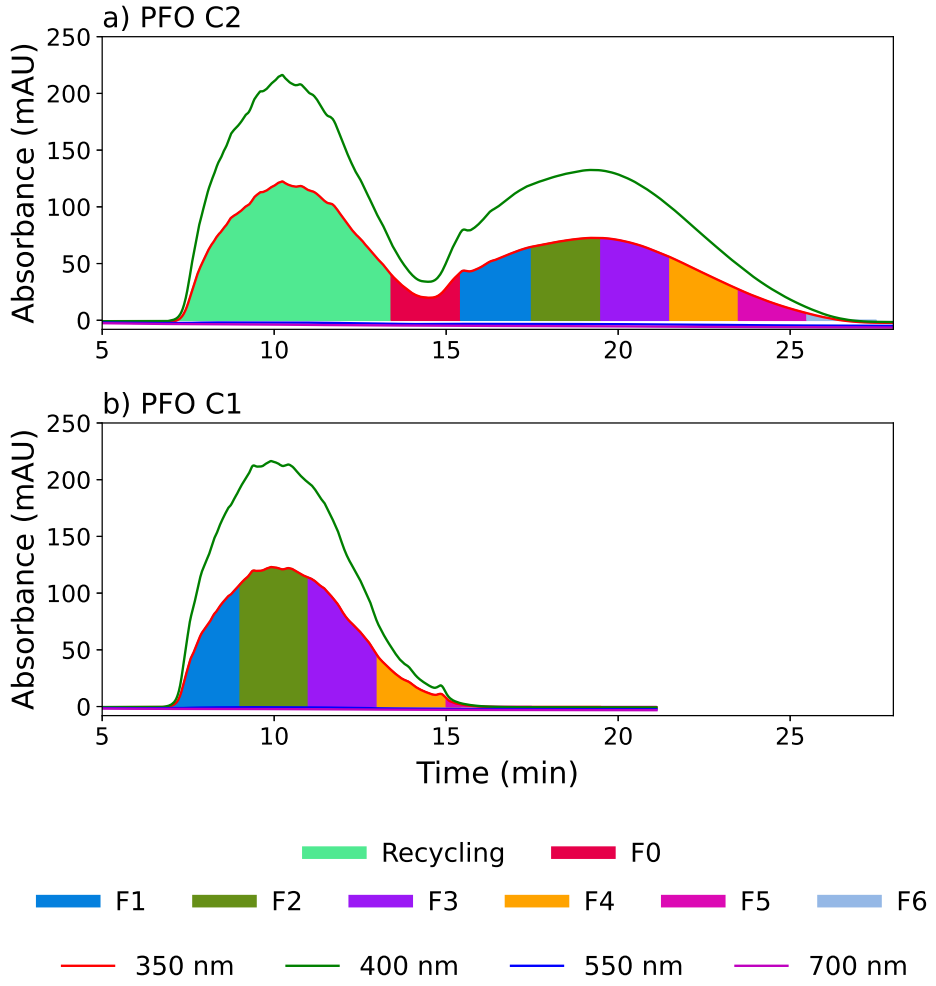

Figure 4.11 | Separation of PFO. *Chromatograms from the two separations of PFO. In a) PFO C2, six fractions were isolated during the second cycle, while b) PFO C1 generated five fractions collected during the first cycle.*

The MW distributions of PFO C2, shown in Figure 4.12a, demonstrate consistent main peaks covering a wide MW range, with M_w from 13 to 533 kDa. F1 contains a relatively long tail towards lower MWs, showing that it is potentially mixed with shorter chains. For F1-F4 there are also smaller peaks around 10^7 Da, suggesting that mixing may have taken place for these fractions. Notably, these peaks are in a similar position to the peak observed in the MW distribution of the neat sample (Figure 4.9).

In order to isolate unmixed fractions, the separation was redone without recycling (PFO C1, Figure 4.11b). This yielded five fractions. Comparing the chromatograms of PFO C2 and PFO C1, the small feature around 15 min is present in both, while it overlaps the second cycle in PFO C2. This implies that the feature originates from the first cycle and is mixed into the second cycle.

As the peak shaving in collection of F0 ends just prior to this feature, some mixing of fractions from PFO C2 would not be unreasonable. Interestingly, however, the

MW distributions of the PFO C1 fractions (Figure 4.12b) reveal similar peaks in the same region, suggesting that the peaks are not solely resulting from mixing due to recycling. In comparison to PFO C2 (Figure 4.12a), the main distributions peaks of PFO are slightly broader, indicating a higher dispersity. Note that F5 from PFO C1 could not be measured as the amount of sample was not sufficient.

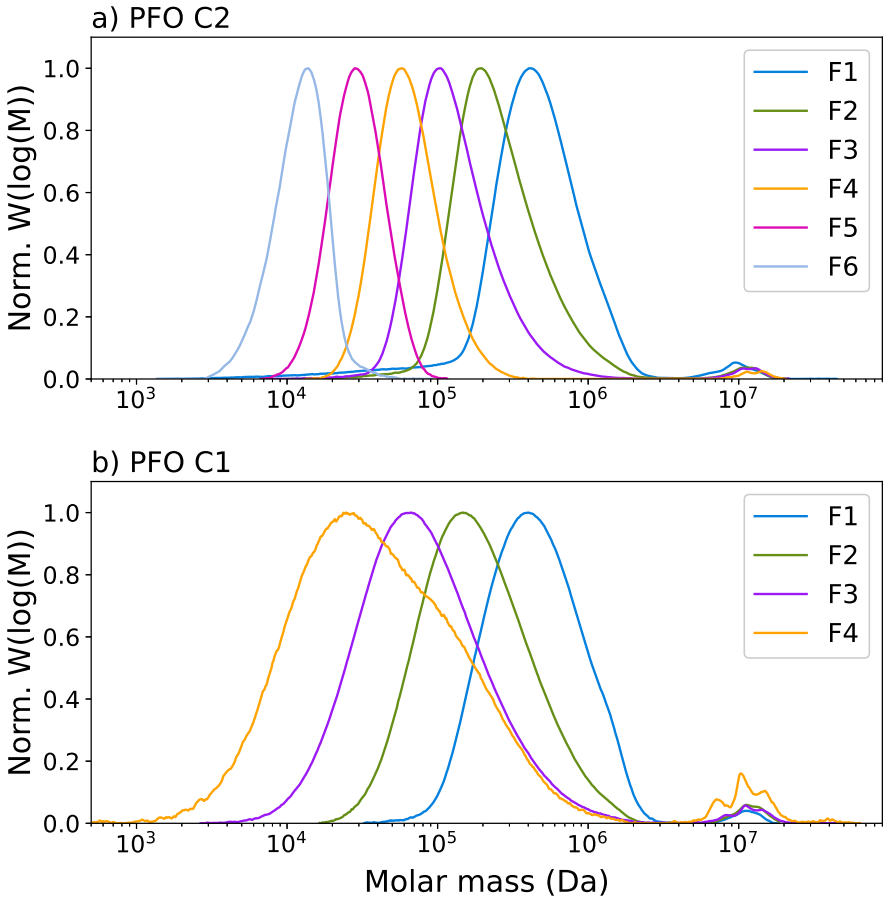

Figure 4.12 | Normalized MW distributions of PFO fractions. *MW distributions of the a) PFO C2 and b) PFO C1 separations. The distributions show smaller peaks around 10^7 Da in some fractions from both separations. Note that F5 from PFO C1 could not be measured as the amount of sample was insufficient.*

The MW distribution data and yields of fractions from PFO C2 and PFO C1 are summarized in Table 4.7. Here, only the main peaks are compared as fractions from both separations showed the smaller peaks. The separations resulted in fractions with a broad MW range, with M_w from 13-551 kDa. Compared to the GPC measurements of the neat PFO (table 4.6, Đ = 3.63), all fractions from PFO C2 showed lower dispersities, with the lowest being F5 and F6, both at 1.18. Đ values of PFO C2 were all below 1.5 with the exception of F1 at 2.35, most likely as it was mixed with low MW polymer. Aside from F1, PFO C1 fractions were more disperse than the corresponding PFO C2 fractions. Regardless, PFO C1 also reduced Đ compared to the neat polymer in all fractions, except for F4 in which Đ was higher at 4.47.

The total yields for the PFO separations were higher than for P3HT at 95% for PFO C2 and 108% for PFO C1. Possibly, the yield exceeding 100% for PFO C1 could stem from traces of solvent, and it it possible that PFO C2 also contains similar traces. Another potential reason is weighing errors. Both separations resulted in higher individual yields for the medium and high MW compared to the low MW fractions, with F2 being the highest at 24% for PFO C2 and 44% for PFO C1. For the lower MW fractions (F5 and F6 for PFO C2, F4 and F5 for PFO C1), yields ranged from 2-9%.

Table 4.7. MW distribution data for main peaks and yields of fractions from PFO separations.

	PFO C2				PFO C1			
	M_n (kDa)	M_w (kDa)	Đ	Yield (%)	M_n (kDa)	M_w (kDa)	Đ	Yield (%)
F0	-	-	-	7	-	-	-	-
F1	227	533	2.35	21	343	551	1.61	20
F2	206	309	1.50	24	131	253	1.94	44
F3	109	158	1.45	21	51	125	2.43	33
F4	57	72	1.26	14	19	86	4.47	9
F5*	27	31	1.18	6	-	-	-	2
F6	11	13	1.18	2	-	-	-	-

*Could not be measured for PFO C1 due to low amount of sample.

Figure 4.13 displays the UV-vis absorption spectra for solutions of all PFO fractions. For both PFO C2 (Figure 4.13a) and PFO C1 Figure (4.13b), the spectra shows absorbance between 300 and 420 nm, with a maximum around 390 nm. No peak is present above 420 nm in addition to the main absorption band, indicating that none of the samples contain β-phase. All fractions demonstrate similar spectra, suggesting similar aggregation behavior between fractions. In general, the absorbance is however blue-shifted slightly with decreasing MW, with more apparent blue-shifts for the lowest MW fractions (F6 for PFO C2, F5 for PFO C1).

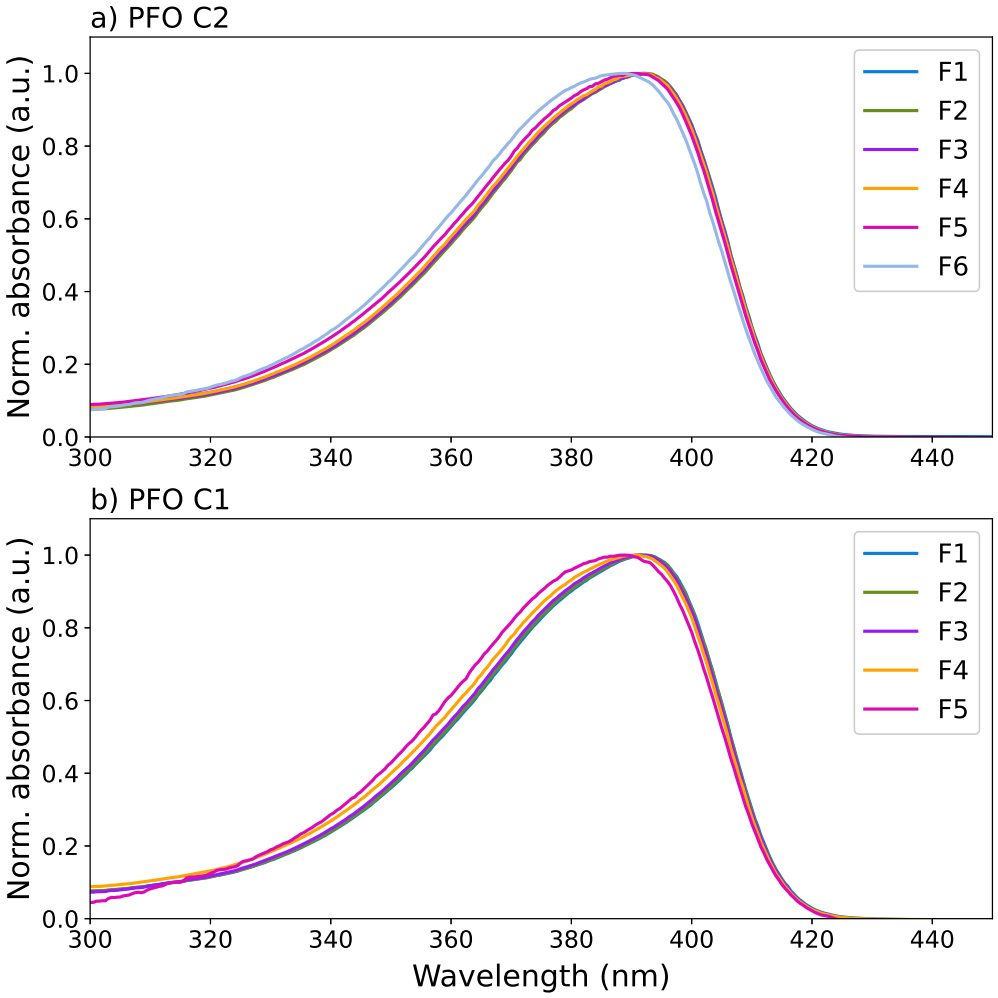

Figure 4.13 | Normalized UV-vis spectra for PFO solutions. *Fractions from a) PFO C2 and b) PFO C1 showed similar absorbance spectra without shoulders or other features.*

5
Discussion

5.1 Significance of recycling

The results show clear indications of how recycling affects the MW distributions of fractions obtained from the separations. In the separations where recycling was not performed (P3HT Neat C1 and PFO C1), fractions were overall more disperse than their counterparts where recycling was carried out (P3HT Neat iteration 1 and 2, and PFO C2). However, the results also demonstrate how recycling can lead to mixing. This is perhaps the most apparent in the separations of F0, where recycling twice in P3HT F0 C3 resulted in heavily mixed distributions for some fractions (Figure 4.8a), even though it provided very low Đ values for the fractions that were not mixed (Table 4.5). More subtle signs of mixing were also observed when recycling was performed, even for fractions with relatively low dispersities. Example of this is F1 from the two iterations of neat P3HT (Figure 4.2) and F1 from PFO C2 (Figure 4.12b), where the shoulders in their lower MW range likely is a result of mixing due to recycling.

These observations highlight the challenge of optimizing HPLC separations when it comes to recycling, both when it comes to number of cycles and peak shaving. Even though peak shaving can be performed to prevent major mixing, as in PFO C2 (Figure 4.11), some degree of mixing may still be difficult to avoid when recycling, if there is an overlap between the peaks of two cycles. Extending the peak shaving interval could potentially prevent even smaller amounts of mixing, although the disadvantage is that this would lower the yields of the remaining fractions. This is likely a limitation of HPLC when performed on even more disperse polymer batches than those studied here, as those will likely have wider HPLC peaks. Recycling could thus induce a major overlap even between the first and second cycles, making peak shaving of a large percentage of the sample necessary to avoid mixing. It may therefore be difficult to achieve low Đ fractions with reasonable yields for these batches, while keeping the same column length.

5.2 Separation of neat P3HT

The two separations of neat P3HT resulted in the isolation of five fractions with nearly identical MW distributions and similar individual yields. Đ was lowered from >2 of the neat polymer for all fractions, down to as low as 1.08. This higlights the performance of the HPLC method in narrowing the dispersity of polymers after it has been optimized. Additionally, the simliar yields and MW distributions of the two iterations demonstrate the reproducibility of the method for P3HT. These promising results show the potential of using HPLC to extract polymers of more

specific chain lengths from a disperse batch containing a wide range of different chain lengths. In a wider perspective, the method could be used to improve polymeric OSCs for electrochemical applications in regards to their microstructure, to facilitate better charge transport and allowing more flexibility in tuning of their mechanical properties. Moreover, the method could potentially be applied to overcome the issues with batch-to-batch variations by enabling the acquisition of similar materials from different batches, supporting the long-term development of electrochemical devices. It should be noted, however, that a limitation of the technique is that the individual yields of fractions will likely vary between batches, as they are dependent on the volume fraction of chain lengths in each batch. For instance, in the separations of neat P3HT, F3 and F4 showed higher yields compared to the other fractions (Table 4.2), resulting from the fact that they are located near the maximum of the neat MW distribution, as seen in Figure 4.2. In the case of separating a different batch where the maximum is shifted, yields will likely increase toward the same direction as the maximum.

Both separations resulted in high total yields of >70%, although this includes F0, which is assumed to have a mixed MW distribution. A total yield of around 60% of unmixed fractions is hence to be expected. The sample preparation is likely where the largest loss of polymer occurs, as polymer solution at high concentration is lost when transferring and filtering the sample. Minor changes to this step could improve the yield slightly, although unlikely by a significant amount. It is also important to note that the concentration and sample preparation should not be varied between repeated separations, as this could impact the reproducibility of the technique. Some material is also lost in the separation itself, as a small amount can be assumed to get remain in the column and get lost during non-collection periods when solvent it pumped through the system. When precipitating the fractions, the amount of chloroform they are redissolved in needs to be minimal as the polymer would not otherwise precipitate in the methanol, consequently leading to some polymer solution being left in the glassware. Furthermore, while filtering the precipitate, polymer is lost in the filtering equipment and, due to its static behavior, during transfer from the filter to the sample vial.

The thin film UV-vis measurements of P3HT fractions showed that decreasing MW generally resulted in more molecular aggregation. This result is expected as shorter chains can organize better and thus contribute to stronger aggregation. As for why F1 did not follow this trend, an explanation could be that the polymer was more oxidized than the other high MW fractions, something that could be explained by its higher absorbance above 650 nm. Moreover, the fact that the spectra were not immensely different between the fractions suggest that the molecular aggregation varies only slightly between them. Since all measured fractions were of relatively high MW - above the range where chains start to entangle, this is also expected as literature suggests that the mechanical properties, including aggregation, do not significantly change above this point.

5.3 Separation of F0

The separations of F0 demonstrate that it is possible to isolate fractions of some of the highest and lowest MW polymer chains in the P3HT batch. The primary goal was to obtain low MW fractions in order to study how the properties of the material change near and below the MW threshold where chain entanglement for P3HT begins. Measurements of F3-F6 from P3HT F0 C2 and F5-F6 from P3HT F0 C3, which are in the number average MW range of 4.1-43 kDa, are particularly relevant for this investigation.

Collection of F0 fractions during the third cycle (P3HT F0 C3) resulted in mixing for some fractions, although Đ were lower for the unmixed fractions compared to the fractions from P3HT F0 C2. This emphasizes both the advantage and disadvantage of recycling - additional cycles can result in lower Đ but come with the risk of mixing. Future work should be focused on investigating if P3HT F0 C3 can be optimized by adjusting the peak shaving interval so that mixing does not occur. This should be done with care, however, as to not throw away low MW polymer - this region is where it is is expected to elute.

Compared to the separations of neat P3HT, the separations of F0 resulted in significantly lower yields at around 50%. This is likely due to the amount of starting material being 6-10 times lower, causing a higher percental loss in each preparation step. Theoretically, P3HT F0 C3 should achieve a lower total yield than P3HT F0 C2 with the same amount of starting material as a result of sending sample to waste to prevent mixing in the former.

Overall, the separations of F0 demonstrate that further separation of fractions into an increased number of fractions can be useful to obtain materials with specific MW distributions. It would also be of interest to attempt further separation of unmixed fractions to investigate how much Đ can be further lowered. The drawback of doing this is that the low yield of each individual fraction could be limiting depending on the type of study to be carried out on the sample, as the availability may not be sufficient for multiple measurements if required.

5.4 Separation of PFO

Overall, the separations of PFO were successful in lowering Đ compared to the measured neat sample. Considering the main peaks, Đ values were generally higher than the P3HT fractions, although this is to be expected as Đ for the neat polymer was higher for PFO than for P3HT. With the exception of F1, collecting fractions during the second cycle in PFO C2 yielded lower Đ of corresponding fractions than collecting during the first cycle in PFO C1, again demonstrating the benefit of recycling. Đ was likely higher for F1 in PFO C2 as it was mixed with some lower MW polymer, as can be seen in its MW distribution in figure 4.12a between 10^4 and 10^5 Da. To prevent this, the interval for F0 could be extended slightly.

In comparison to P3HT, higher M_n and M_w values were observed in the PFO fractions, particularly for those of high MW. As the neat PFO also showed higher values than the neat P3HT, this is expected. Yet, because PFO has a higher l_p than P3HT, its MW is likely more overestimated, meaning this result cannot be used to directly compare chain lengths between the two polymers. PFO was reported to be overestimated by 2.7 times in one study [24], hence the overestimation for P3HT should be less than this. Moreover, this number suggests that the overestimation factor is not proportional to l_p, as the latter is 7-9 times higher for PFO compared to PS. Exploring the relationship between l_p and overestimation could be of interest for future work.

The total yields for the PFO separations were higher than for P3HT. Apart from the suspected solvent traces, another reason to why the yields were higher than for P3HT may include the lower concentration of the HPLC sample, reducing the amount of polymer lost in the transferring and filtering step as well as in the HPLC instrument. A major factor that could have more significant influences on the yield is that PFO may interact more strongly with the stationary phase and is therefore lost during non-collection periods where the pump is flowing. Consequently, direct comparisons of the yields obtained from separating different polymers is challenging.

It is unclear what causes the smaller peaks in the measured MW distributions for PFO. Normally, mixed distributions only arise as a result of recycling, although the peaks were also present for the PFO C1 fractions where recycling was not performed. Consequently, it is plausible that the peaks originate from something else. A possible reason is that a small portion of polymer chains in the MW range of the main peaks form larger aggregates in solution, either by intermolecular aggregation or deviating conformations in individual chains, for example β-phase formation. This could delay their from the column compared to chains of similar length. As for why the small peak was not resolved separately in the HPLC chromatograms, an explanation could be that the higher concentration or other variations in conditions affects the formation of aggregates. Further experiments that can determine the microstructure and conformation of the polymer, such as grazing incidence wide angle x-ray scattering (GIWAXS) measurements and UV-vis measurements on solutions of varying concentrations, could be used to support this hypothesis.

Considering the main peaks, the fractions of PFO C2 demonstrated relatively low Đ and covered a wide range of MWs between M_w = 13-533 kDa. Thus, it could be interesting to explore whether these fractions could be used as a new calibration standard for analytical GPC MW measurements, by extracting their absolute M_w using SLS. Ideally, however, more fractions with even lower Đ should be obtained to ensure that the calibration curve accurately represents MWs across the entire calibration range. As the current PS standard includes 12 data points with Đ $<$ 1.1, this could serve as a target to aim for. One way to do this could be to lower the time interval between fraction collections. A suggestion is to slightly prolong the collection interval for F0 to lower Đ of F1, as explained, followed by collecting fractions in 1 minute intervals. As the total time for fraction collection is currently around 12 min (15.5-27.5 min), this procedure should yield 10-12 fractions.

The UV-vis absorption spectra were similar for all PFO fractions, although with a slight blue-shift with decreasing MW. This blue-shift likely originates from the fact that a lower MW results in a lower hydrodynamic volume, causing a shift in absorbance. Nevertheless, the similarities between the spectra suggest similar aggregation in the different samples. Further measurements with different concentrations would however need to be performed to asses β-phase formation and whether the samples are aggregated or not. By varying the concentration and observing differences in the spectra, such as if shoulders or other features appear, indications of the aggregation states could be obtained. A low degree of aggregation is beneficial when performing SLS measurements to assess the absolute M_w of fractions, as the goal here is to measure individual polymer chains. Thin film measurements could also be of interest for PFO samples future studies to investigate if the solid-state aggregation is also similar between the fractions.

5.5 NMR vs GPC for measuring MW

Comparing NMR to GPC in determining DP_n and M_n, GPC provided much higher values, showing how GPC likely overestimates the MW for P3HT when it is measured relative to PS, due to its increased stiffness compared to the latter. The NMR values were slightly lower than expected, especially for the high MW fractions. Literature reported that GPC overestimated the MW of PFO by up to a factor of 2.7 [24]. As PFO has a much higher l_p compared to P3HT (Table 2.1), this means that the MW measured with GPC should be overestimated by less than 2.7 times for P3HT. Since NMR provided more than five times higher values than GPC for some fractions, it likely underestimated DP_n and M_n in this case, and the actual values should lie somewhere in between those determined via the two techniques.

One factor that could cause the underestimation of NMR is the presence of regioirregularities, i.e. disorder in the head-tail arrangement of the repeating units in the polymer chains. These irregularities likely change the chemical shift of the studied protons, excluding them from the measurements. Because these protons are located in the repeating units of the main chain, this results in an underestimation. Another factor that causes inaccuracies are that the peaks are sometimes overlapping and poorly resolved. Even when peaks are well resolved, it can be difficult to determine what protons they correspond to. It is also not known whether the end groups are H/H or H/Br, or a mixture of the two. Defining the integration ranges is therefore challenging as the peak boundaries are not apparent, and the integration ranges have a relatively strong influence on the result. Although the errors caused by regioirregularities are difficult to prevent, the others may potentially be reduced by using a higher polymer concentration or a different solvent.

Investigating the accuracy of NMR for measuring other polymers than P3HT could be of interest for future studies. A requirement for this, if a similar end group analysis is to be carried out, is that the end groups contain one or more protons that show a different chemical shift compared to a set of protons in the main chain. These protons must also show well-resolved peaks with no overlap to ensure accurate

measurements. Polymers must also be prepared with high regioregularity, preferably >99%, so that all repeating units in the main chains are represented in the main chain peak.

6

Conclusions and future outlook

In summary, this study investigated the use of preparative HPLC to separate disperse polymeric OSC samples into less disperse fractions of varying MWs. The method was firstly developed using the well-studied P3HT and applied to PFO after optimization, with the goal of isolating fractions for use as alternative calibration standards for GPC. Separations were conducted with varying recycling and fraction collection conditions to explore how these factors influenced the MW distributions of the obtained fractions. For thin films of P3HT and solutions of PFO with different MW distributions, the molecular aggregation behavior was studied through UV/vis measurements. Moreover, GPC was compared to NMR in determining the MW of P3HT.

For both P3HT and PFO, the method showed promising results. In the majority of the obtained fractions after optimization, Đ was significantly lowered compared to the neat polymer, fractions were of varying MW, and the total yields were reasonable. Moreover, its reproducibility was demonstrated for P3HT, for which two repeated iterations resulted in nearly identical fractions. The separations of F0 also illustrated, that HPLC can be used to acquire polymer fractions of relatively specific chain lengths, although a limitation of the technique is that individual yields can sometimes be low due to the chain fraction volume of the polymer batch.

The results furthermore indicated that recycling can be used to lower Đ of fractions, though another limitation is that mixing can be difficult to avoid when it is performed. Peak shaving can be implemented to prevent some degree of mixing, although it leads to lower yields of the remaining fractions and may not be sufficient if the overlap between cycles is large. A possible way of overcoming this, however, is to decrease the time intervals of fraction collections. Future work could investigate how this would influence the MW distributions of fractions.

The comparison between GPC and NMR highlighted the inaccuracies in these typical MW determination methods for polymeric OSCs. Thus, the main continuation on this project should focus on the use of HPLC to develop alternative calibration standards to ensure more precise GPC measurements of these polymers. The fractions of PFO C2 could serve as a basis for such a study. It is however of importance to disclose what is causing the smaller peaks in their MW distributions, and whether they impact the performance of the fractions when used as standards. Optimization may also include isolating more fractions with even more narrow dispersites compared to those obtained in this study. If PFO proves successful as a calibration standard, further studies could also investigate the possibility of developing standards of other polymers with varying l_p.

In a wider perspective, this work shows the potential of HPLC in improving our understanding of polymeric OSCs. By extending the knowledge of the technique to also

facilitate the removal of metal impurities and minimize variations between batches, it could assist the development of metal-free electronic devices for applications such as batteries, solar cells, elecrochemical synthesis and sensors.

References

[1] Matthew Leech and Kevin C.Lam. "A practical guide to electrosynthesis". In: *Nature Reviews Chemistry* 6 (2022), pp. 275–286. DOI: 10.1038/s41570-022-00372-y.

[2] Bryan D. Paulsen et al. "Organic mixed ionic–electronic conductors". In: *Nature Materials* 19 (2020).

[3] Ana De La Fuente Durán et al. "Origins of hydrogen peroxide selectivity during oxygen reduction on organic mixed ionic–electronic conducting polymers". In: *Energy Environ. Sci.* 16 (11 2023), pp. 5409–5422.

[4] Carolyn Gramling. "Rare earth mining may be key to our renewable energy future. But at what cost?" In: *ScienceNews* (2023).

[5] Philip Rohland et al. "Redox-active polymers: The magic key towards energy storage – a polymer design guideline progress in polymer science". In: *Progress in Polymer Science* 125 (2022), p. 101474. ISSN: 0079-6700. DOI: https://doi.org/10.1016/j.progpolymsci.2021.101474.

[6] Hugo Bronstein et al. "The role of chemical design in the performance of organic semiconductors". In: *Nature Reviews Chemistry* 4 (2020), pp. 66–77.

[7] Samuel J. Ling, Jeff Sanny, and William Moebs. *University Physics*. Vol. 3. Massachusetts: OpenStax, 2016. Chap. 9.4: Semiconductors and Doping.

[8] Rodrigo Noriega et al. "A general relationship between disorder, aggregation and charge transport in conjugated polymers". In: *Nature materials* 12 (2013), pp. 1038–1044.

[9] Maximilian Moser et al. "Materials in Organic Electrochemical Transistors for Bioelectronic Applications: Past, Present, and Future". In: *Advanced Functional Materials* 29.21 (2019), p. 1807033. DOI: https://doi.org/10.1002/adfm.201807033. URL: https://advanced.onlinelibrary.wiley.com/doi/abs/10.1002/adfm.201807033.

[10] Siew Ting Melissa Tan et al. "Redox-Active Polymers Designed for the Circular Economy of Energy Storage Devices". In: *ACS Energy Letters* 6.10 (2021), pp. 3450–3457. DOI: 10.1021/acsenergylett.1c01625. eprint: ttps://doi.org/10.1021/acsenergylett.1c01625. URL: https://doi.org/10.1021/acsenergylett.1c01625.

[11] Nezha Badi, Delphine Chan-Seng, and Jean-François Lutz. "Microstructure Control: An Underestimated Parameter in Recent Polymer Design". In: *Macromolecular Chemistry and Physics* 214.2 (2013), pp. 135–142. DOI: https://doi.org/10.1002/macp.201200475. eprint: https://onlinelibrary.wiley.com/doi/pdf/10.1002/macp.201200475. URL: https://onlinelibrary.wiley.com/doi/abs/10.1002/macp.201200475.

[12] Ronald W. Nunes, John R. Martin, and Julian F. Johnson. "Influence of molecular weight and molecular weight distribution on mechanical properties of polymers". In: *Polymer Engineering & Science* 22.4 (1982), pp. 205–228. DOI: https://doi.org/10.1002/pen.760220402. URL: https://4spepublications.onlinelibrary.wiley.com/doi/abs/10.1002/pen.760220402.

[13] Luyao Lu et al. "Mechanistic Studies of Effect of Dispersity on the Photovoltaic Performance of PTB7 Polymer Solar Cells". In: *Chemistry of Materials* 27.2 (2015), pp. 537–543. DOI: 10.1021/cm5042953. eprint: https://doi.org/10.1021/cm5042953. URL: https://doi.org/10.1021/cm5042953.

[14] Ossila. *P3HT*. URL: https://www.ossila.com/products/p3ht (visited on 03/11/2025).

[15] Yongrui He, Lijun Huo, and Bing Zheng. "Advances of batch-variation control for photovoltaic polymers". In: *Nano Energy* 123 (2024), p. 109397. ISSN: 2211-2855. DOI: https://doi.org/10.1016/j.nanoen.2024.109397. URL: https://www.sciencedirect.com/science/article/pii/S2211285524001459.

[16] Nicholas M. Randell et al. "Effect of Acceptor Unit Length and Planarity on the Optoelectronic Properties of Isoindigo–Thiophene Donor–Acceptor Polymers". In: *Chemistry of Materials* 30.14 (2018), pp. 4864–4873. DOI: 10.1021/acs.chemmater.8b02535. eprint: https://doi.org/10.1021/acs.chemmater.8b02535. URL: https://doi.org/10.1021/acs.chemmater.8b02535.

[17] Sophie Griggs et al. "The effect of residual palladium on the performance of organic electrochemical transistors". In: *Nature Communications* 13 (2022), p. 7964. DOI: 10.1038/s41467-022-35573-y. URL: https://doi.org/10.1038/s41467-022-35573-y.

[18] Alexander Giovannitti et al. "Energetic Control of Redox-Active Polymers toward Safe Organic Bioelectronic Materials". In: *Advanced Materials* 32.16 (2020), p. 1908047. DOI: https://doi.org/10.1002/adma.201908047. URL: https://advanced.onlinelibrary.wiley.com/doi/abs/10.1002/adma.201908047.

[19] Jessika Öhberg. "Purification of conjugated polymers - Better polymers through HPLC purification and Soxhlet extraction". MA thesis. Chalmers University of Technology, 2024.

[20] Manon Denis. "Purification of conjugated polymers using High Performance Liquid Chromatography (HPLC)". MA thesis. Chalmers University of Technology, 2024.

[21] Julia Wollmann et al. “Versatile Approach to Well-Defined Oligofluorenes and Polyfluorenes with Low Dispersity”. In: *Macromolecules* 53.22 (2020), pp. 10137–10146. DOI: 10.1021/acs.macromol.0c01887. eprint: https://doi.org/10.1021/acs.macromol.0c01887. URL: https://doi.org/10.1021/acs.macromol.0c01887.

[22] Jasmeen Sidana and Lokesh Kumar Joshi. “Recycle HPLC: A Powerful Tool for the Purification of Natural Products”. In: *Chromatography Research International* 2013.1 (2013), p. 509812. DOI: https://doi.org/10.1155/2013/509812. eprint: https://onlinelibrary.wiley.com/doi/pdf/10.1155/2013/509812. URL: https://onlinelibrary.wiley.com/doi/abs/10.1155/2013/509812.

[23] Justin J. Kwok et al. “Understanding Solution State Conformation and Aggregate Structure of Conjugated Polymers via Small Angle X-ray Scattering”. In: *Macromolecules* 55.11 (2022), pp. 4353–4366. DOI: 10.1021/acs.macromol.1c02449. eprint: https://doi.org/10.1021/acs.macromol.1c02449. URL: https://doi.org/10.1021/acs.macromol.1c02449.

[24] M. Grell et al. “Chain geometry, solution aggregation and enhanced dichroism in the liquidcrystalline conjugated polymer poly(9,9-dioctylfluorene)”. In: *Acta Polymerica* 49.8 (1998), pp. 439–444. DOI: https://doi.org/10.1002/(SICI)1521-4044(199808)49:8<439::AID-APOL439>3.0.CO;2-A. eprint: https://onlinelibrary.wiley.com/doi/pdf/10.1002/%28SICI%291521-4044%28199808%2949%3A8%3C439%3A%3AAID-APOL439%3E3.0.CO%3B2-A. URL: https://onlinelibrary.wiley.com/doi/abs/10.1002/%28SICI%291521-4044%28199808%2949%3A8%3C439%3A%3AAID-APOL439%3E3.0.CO%3B2-A.

[25] Ryan A. Fair et al. “Molecular Weight Characterization of Conjugated Polymers Through Gel Permeation Chromatography and Static Light Scattering”. In: *ACS Applied Polymer Materials* 3.9 (2021), pp. 4572–4578. DOI: 10.1021/acsapm.1c00647. URL: https://doi.org/10.1021/acsapm.1c00647.

[26] Andrew T. Kleinschmidt, Samuel E. Root, and Darren J. Lipomi. “Poly(3-hexylthiophene) (P3HT): fruit fly or outlier in organic solar cell research?” In: *J. Mater. Chem. A* 5 (23 2017), pp. 11396–11400. DOI: 10.1039/C6TA08317J. URL: http://dx.doi.org/10.1039/C6TA08317J.

[27] Lichun Niu et al. “Insights into the β-phase of polyfluorene: characterization, regulation, and mechanism”. In: *Journal of Polymer Science* 62.3 (2024), pp. 463–479. DOI: https://doi.org/10.1002/pol.20230679. eprint: https://onlinelibrary.wiley.com/doi/pdf/10.1002/pol.20230679. URL: https://onlinelibrary.wiley.com/doi/abs/10.1002/pol.20230679.

[28] Brooke Kuei and Enrique D. Gomez. “Chain conformations and phase behavior of conjugated polymers”. In: *Soft Matter* 13 (1 2017), pp. 49–67. DOI: 10.1039/C6SM00979D. URL: http://dx.doi.org/10.1039/C6SM00979D.

[29] Zhiqiang Cao et al. “Molecular Structure and Conformational Design of Donor-Acceptor Conjugated Polymers to Enable Predictable Optoelectronic Property”. In: *Advanced Materials* 35.41 (2023), p. 2302178. DOI: https://doi.org/10.1002/adma.202302178. eprint: https://advanced.onlinelibrary.wiley.com/doi/pdf/10.1002/adma.202302178. URL: https://advanced.onlinelibrary.wiley.com/doi/abs/10.1002/adma.202302178.

[30] James H. Bannock et al. “Rapid flow-based synthesis of poly(3-hexylthiophene) using 2-methyltetrahydrofuran as a bio-derived reaction solvent”. In: *European Polymer Journal* 80 (2016), pp. 240–246. ISSN: 0014-3057. DOI: https://doi.org/10.1016/j.eurpolymj.2016.04.016. URL: https://www.sciencedirect.com/science/article/pii/S0014305716302725.

[31] Ossila. *PFO (F8)*. URL: https://www.ossila.com/products/pfo-f8-19456-48-5?_pos=1&_sid=cd73661e1&_ss=r (visited on 05/14/2025).

[32] Dushanthi S. Dissanayake et al. “Determination of absolute molecular weight of regioregular poly(3-hexylthiophene) by 1H-NMR analysis”. In: *Journal of Polymer Science Part A: Polymer Chemistry* 55.1 (2017), pp. 79–82. DOI: https://doi.org/10.1002/pola.28354. eprint: https://onlinelibrary.wiley.com/doi/pdf/10.1002/pola.28354. URL: https://onlinelibrary.wiley.com/doi/abs/10.1002/pola.28354.

[33] Xin Guo, Martin Baumgarten, and Klaus Müllen. “Designing π-conjugated polymers for organic electronics”. In: *Progress in Polymer Science* 38.12 (2013). Topical issue on Conductive Polymers, pp. 1832–1908. ISSN: 0079-6700. DOI: https://doi.org/10.1016/j.progpolymsci.2013.09.005. URL: https://www.sciencedirect.com/science/article/pii/S0079670013001196.

[34] Kirsten Bruchlos et al. “Poly(3-hexylthiophene) revisited – Influence of film deposition on the electrochemical behaviour and energy levels”. In: *Electrochimica Acta* 269 (2018), pp. 299–311. ISSN: 0013-4686. DOI: https://doi.org/10.1016/j.electacta.2018.02.126. URL: https://www.sciencedirect.com/science/article/pii/S0013468618304316.

[35] Edward J. W. Crossland et al. “Systematic Control of Nucleation Density in Poly(3-Hexylthiophene) Thin Films”. In: *Advanced Functional Materials* 21.3 (2011), pp. 518–524. DOI: https://doi.org/10.1002/adfm.201001682. eprint: https://advanced.onlinelibrary.wiley.com/doi/pdf/10.1002/adfm.201001682. URL: https://advanced.onlinelibrary.wiley.com/doi/abs/10.1002/adfm.201001682.

[36] Long Huang et al. “Study of β phase and Chains Aggregation Degrees in Poly(9,9-dioctylfluorene) (PFO) Solution”. In: *The Journal of Physical Chemistry C* 116.14 (2012), pp. 7993–7999. DOI: 10.1021/jp301102t. eprint: https://doi.org/10.1021/jp301102t. URL: https://doi.org/10.1021/jp301102t.

[37] Michael W. Dong. *Modern HPLC for practicing scientists*. John Wiley & Sons, Inc., 2006.

[38] Thermo Fisher Scientific Inc. *How HPLC Detectors Work*. URL: https://www.thermofisher.com/se/en/home/industrial/chromatography/chromatography-learning-center/liquid-chromatography-information/hplc-system-components/how-hplc-detectors-work.html?erpType=Global_E1 (visited on 07/05/2025).

[39] Aijiren. *What is the difference between analytical and preparative HPLC?* https://www.hplcvials.com/knowledge/analytical-vs-preparative-hplc-understanding-key-differences.html. Accessed: 2025-06-08. 2024.

[40] Scott P. O. Danielsen, Colin R. Bridges, and Rachel A. Segalman. "Chain Stiffness of Donor–Acceptor Conjugated Polymers in Solution". In: *Macromolecules* 55.2 (2022), pp. 437–449. DOI: 10.1021/acs.macromol.1c02229. eprint: https://doi.org/10.1021/acs.macromol.1c02229. URL: https://doi.org/10.1021/acs.macromol.1c02229.

[41] G.D. Wignall, D.G.H. Ballard, and J. Schelten. "Measurements of persistence length and temperature dependence of the radius of gyration in bulk atactic polystyrene". In: *European Polymer Journal* 10.9 (1974), pp. 861–865. ISSN: 0014-3057. DOI: https://doi.org/10.1016/0014-3057(74)90142-6. URL: https://www.sciencedirect.com/science/article/pii/0014305774901426.

[42] Hwankyu Lee et al. "Molecular Dynamics Studies of Polyethylene Oxide and Polyethylene Glycol: Hydrodynamic Radius and Shape Anisotropy". In: *Biophysical Journal* 95.4 (2008), pp. 1590–1599. ISSN: 0006-3495. DOI: https://doi.org/10.1529/biophysj.108.133025. URL: https://www.sciencedirect.com/science/article/pii/S0006349508701255.

[43] Malvern Instruments Limited. *Static Light Scattering technologies for GPC SEC explained*. white paper. Accessed: 2025-06-18. Grovewood Road, Malvern, Worcestershire, UK. WR14 1XZ: Malvern Instruments Limited, 2015. URL: https://www.chem.uci.edu/~dmitryf/manuals/Fundamentals/SLS%20Technologies%20GPC-SEC%20Explained.pdf.

[44] Naga Rajesh Tummala et al. "Entanglements in P3HT and their influence on thin-film mechanical properties: Insights from molecular dynamics simulations". In: *Journal of Polymer Science Part B: Polymer Physics* 53.13 (2015), pp. 934–942. DOI: https://doi.org/10.1002/polb.23722. URL: https://onlinelibrary.wiley.com/doi/abs/10.1002/polb.23722.

A

Appendix A: Separation event times

Tables A.1-A.6 show the time intervals for recycling and fraction collection for all HPLC separations.

Table A.1. Recycling and collection protocol for P3HT Neat iteration 1 and 2. The protocol was repeated three times (once for each injection).

Event	From [min]	To [min]
Recycle 1	8.589	13.589
F0	13.600	18.690
Recycle 2	18.700	26.089
F1	27.500	29.500
F2	29.510	31.499
F3	31.510	33.499
F4	33.510	35.499
F5	35.510	37.499

Table A.2. Recycling and collection protocol for the separation of neat P3HT without recycling.

Event	From [min]	To [min]
F1	8.589	10.589
F2	10.599	12.589
F3	12.600	14.589
F4	14.600	16.589

Table A.3. Recycling and collection protocol for P3HT F0 C3.

Event	From [min]	To [min]
Recycle 1	3.822	4.118
Recycle 2	7.958	15.445
Recycle 3	15.886	28.944
F1	31.497	33.492
F2	33.495	35.523
F3	35.525	37.501
F4	37.503	39.496
F5	39.498	41.502
F6	41.505	43.513

Table A.4. Recycling and collection protocol for P3HT F0 C2.

Event	From [min]	To [min]
Recycle 1	7.793	17.069
F1	17.070	19.086
F2	19.088	21.081
F3	21.083	23.079
F4	23.080	25.089
F5	25.092	27.092
F6	27.095	29.080

Table A.5. Recycling and collection protocol for PF0 C2.

Event	From [min]	To [min]
Recycle 1	7.146	13.403
F0	13.403	15.420
F1	15.422	17.479
F2	17.482	19.495
F3	19.497	21.500
F4	21.504	23.497
F5	23.498	25.484
F6	25.487	27.497

Table A.6. Recycling and collection protocol for PF0 C1.

Event	From [min]	To [min]
F1	6.995	9.008
F2	9.010	10.992
F3	10.995	12.998
F4	13.000	15.002
F5	15.003	16.998

B

Appendix B: Supplementary chromatograms

Figure B.1 shows the two full chromatograms, including all three repeat injections from the two repeat separations of neat P3HT.

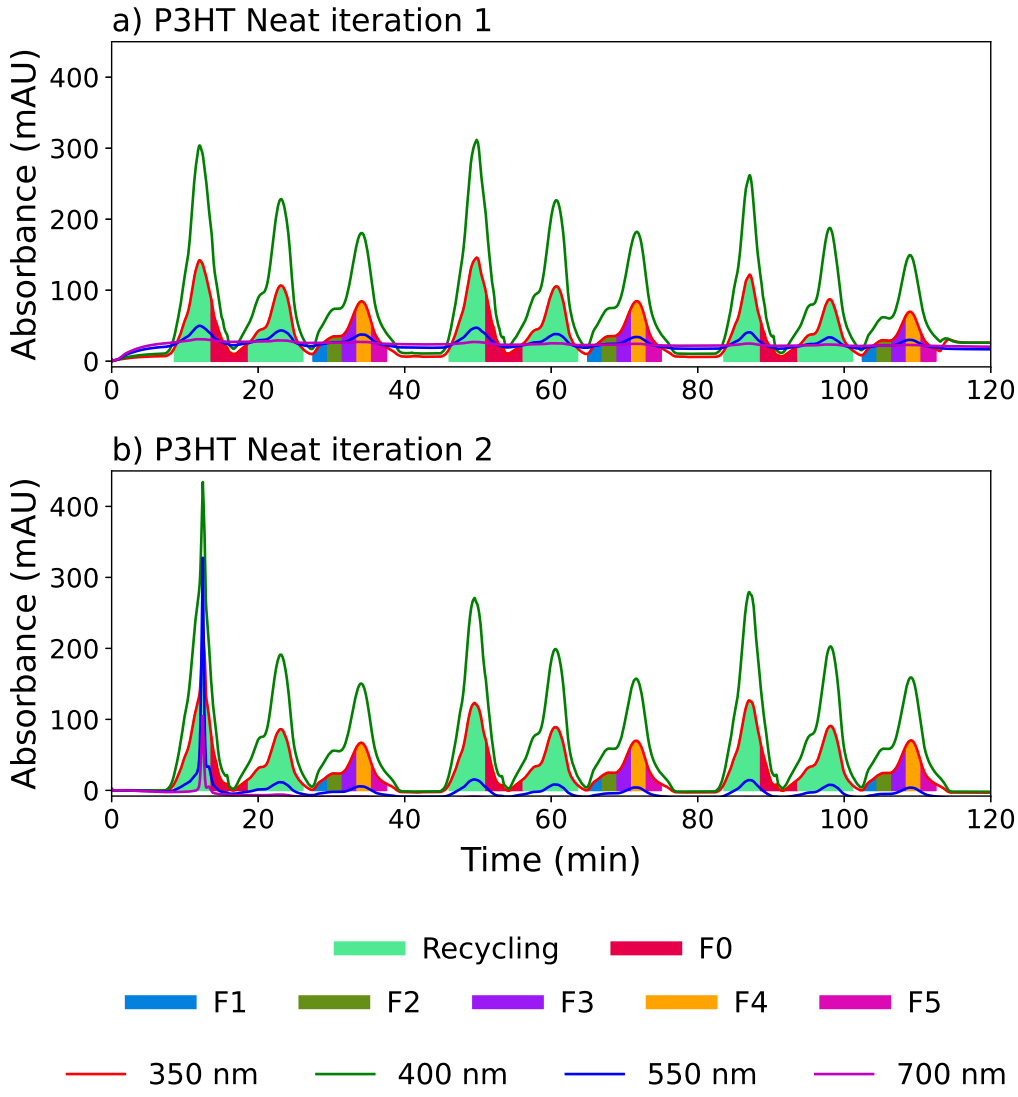

Figure B.1 | Complete chromatograms from P3HT Neat a) iteration 1 and b) iteration 2, showing all three repeat injections.

C

Appendix C: NMR Spectra

Figures C.1-C.5 show the NMR-spectra of thin-film fractions from P3HT Neat iteration 2, zoomed into the peaks that were used to determine DP_n. The green lines at the bases of the peaks represent the applied integration ranges.

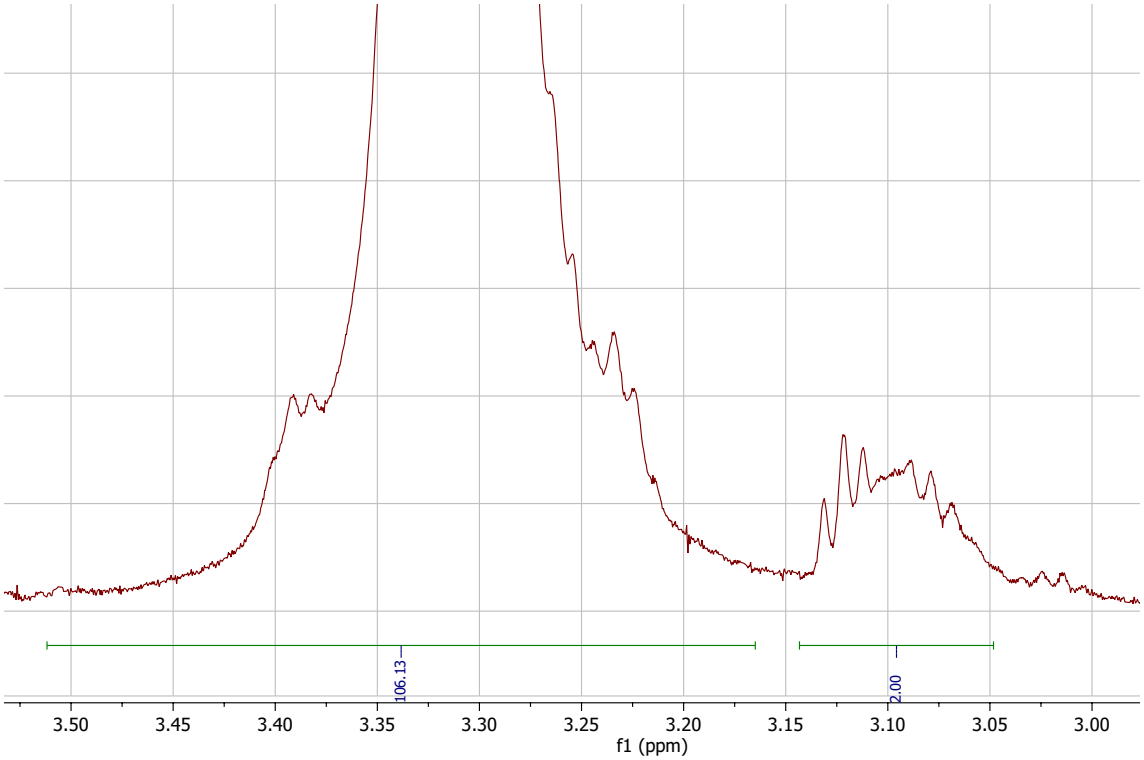

Figure C.1 | Zoomed-in NMR spectra of F1 from P3HT Neat iteration 2

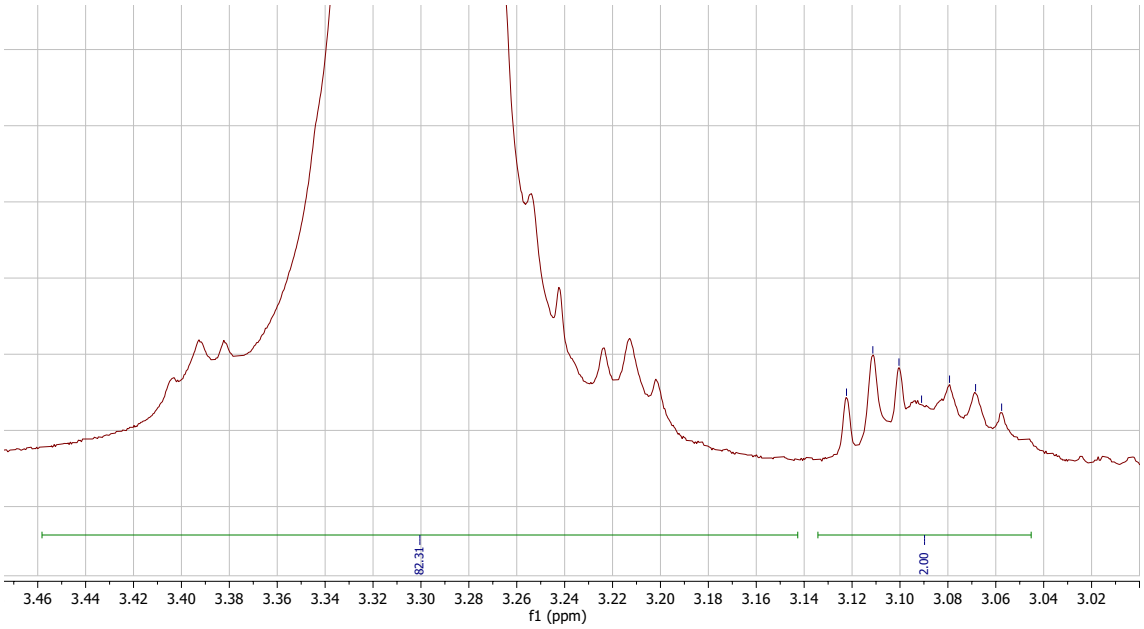

Figure C.2 | Zoomed-in NMR spectra of F2 from P3HT Neat iteration 2

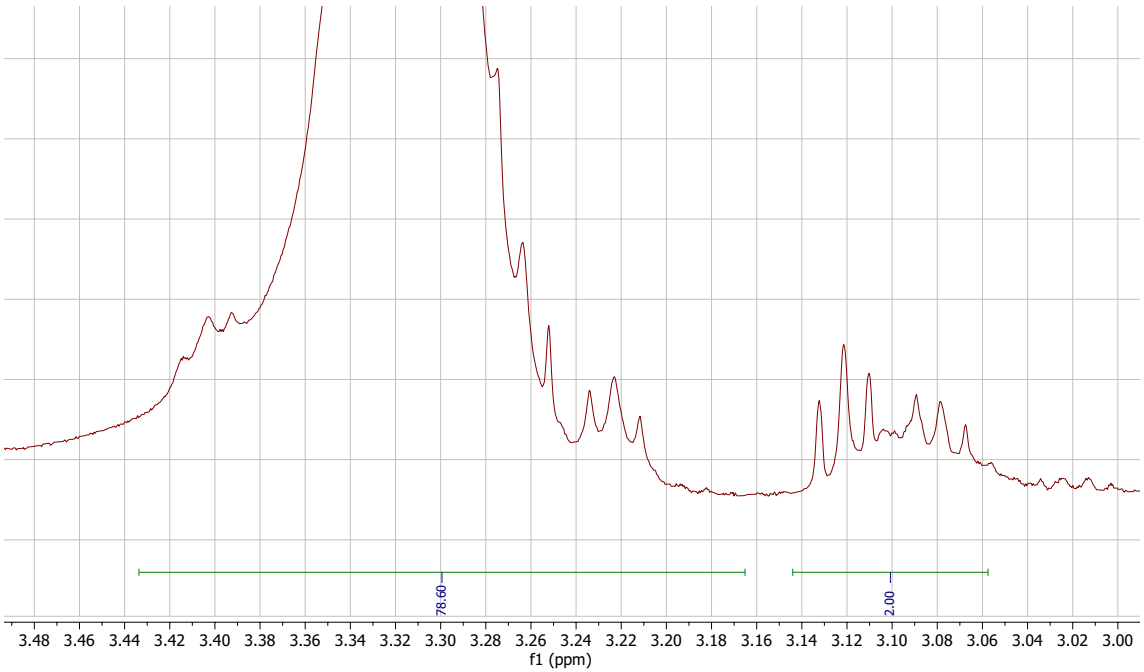

Figure C.3 | Zoomed-in NMR spectra of F3 from P3HT Neat iteration 2

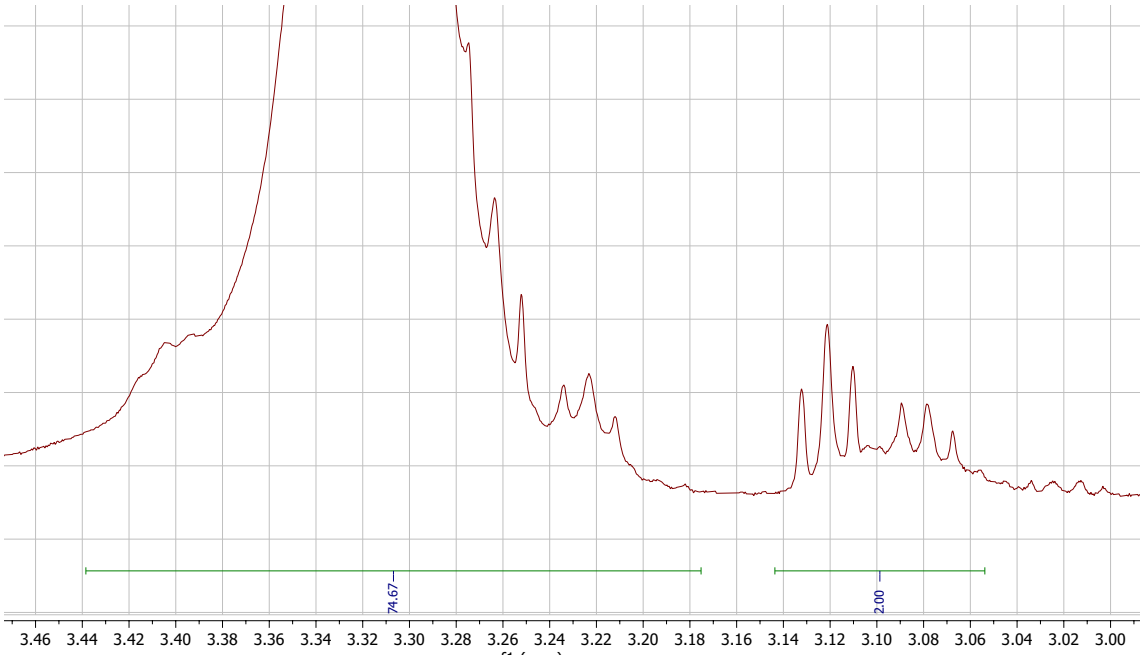

Figure C.4 | Zoomed-in NMR spectra of F4 from P3HT Neat iteration 2

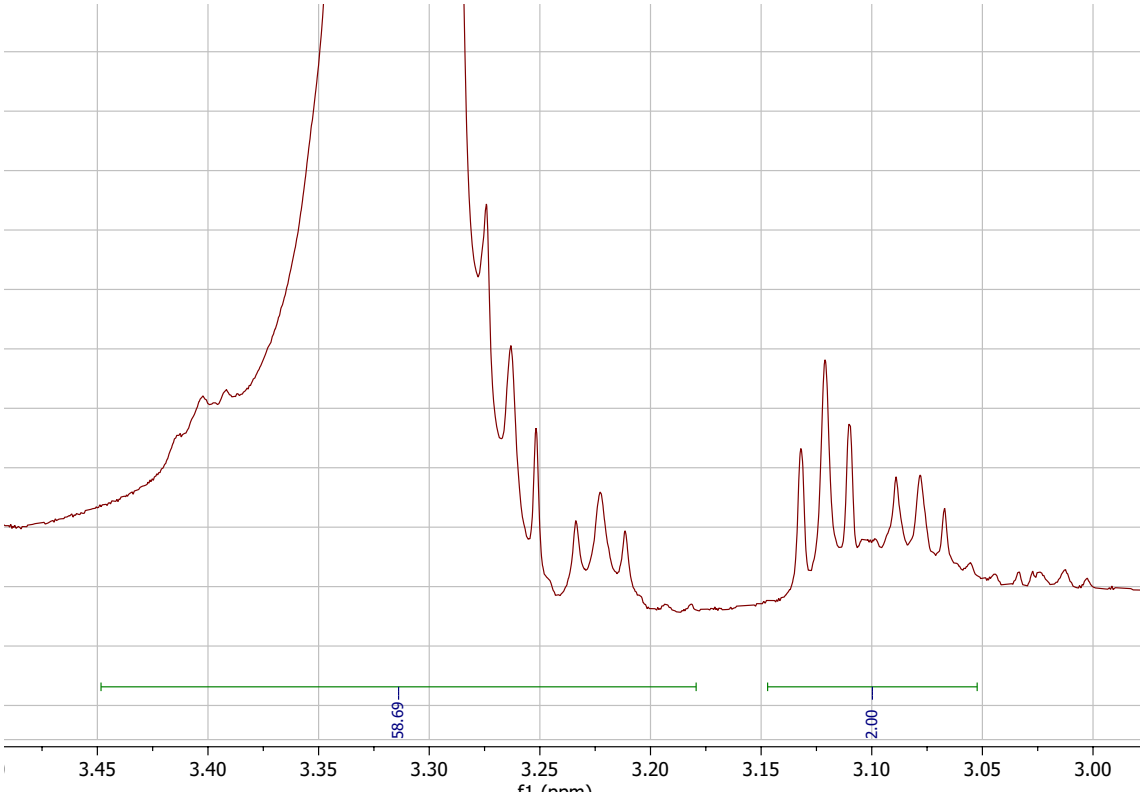

Figure C.5 | Zoomed-in NMR spectra of F5 from P3HT Neat iteration 2

DEPARTMENT OF SOME SUBJECT OR TECHNOLOGY
CHALMERS UNIVERSITY OF TECHNOLOGY
Gothenburg, Sweden
www.chalmers.se

CHALMERS
UNIVERSITY OF TECHNOLOGY